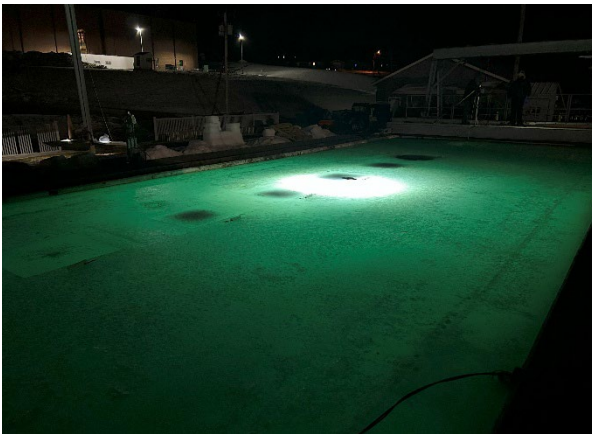


Bureau of Safety and Environmental Enforcement Oil Spill Preparedness Division Detecting Oil Under Ice and On the Seafloor

Final Report

April 2025



(Photos: SL Ross (left) and ARA (right), 2024)

**James McCourt, Craig McNeil, Aaron Marburg, David
Dickins, Nicolas Michel-Hart**

**US Department of the Interior
Bureau of Safety and Environmental Enforcement
Oil Spill Preparedness Division**



Detecting Oil Under Ice and On the Seafloor

Final Report

OSRR # 1155

April 2025

Authors:

James McCourt
SL Ross Environmental Research Ltd.



Craig McNeil, Aaron Marburg, Nicolas Michel-Hart
University of Washington, Applied Physics Laboratory



David Dickins
DF Dickins Associates LLC



Prepared under Contract Number 140E0122C0008
By
SL Ross Environmental Research Ltd.
200-38 Auriga Drive, Ottawa, ON, Canada, K2E 8A5

**US Department of the Interior
Bureau of Safety and Environmental Enforcement
Oil Spill Preparedness Division**



DISCLAIMER

This study was funded by the Bureau of Safety and Environmental Enforcement (BSEE), U.S. Department of the Interior, Washington, D.C., under Contract 140E0122C0008. This final report has been reviewed by the Bureau of Safety and Environmental Enforcement and approved for publication. Approval does not signify that the contents necessarily reflect the views and policies of the BSEE, nor does mention of the trade names or commercial products constitute endorsement or recommendation for use.

REPORT AVAILABILITY

The PDF file for this report is available through the following sources. Click on the URL and enter the appropriate search term to locate the PDF:

Document Source	Search Term	URL
Bureau of Safety and Environmental Enforcement (BSEE)	Project Number – 1155	https://www.bsee.gov/oil-spill-detection-under-ice-and-on-seafloor
U.S. Department of the Interior Library	Detecting Oil Under Ice and On the Seafloor	https://library.doi.gov/uhtbin/cgisirsi/?ps=8L0mpW5uPV/SIRSI/X/60/495/X
National Technical Reports Library	Detecting Oil Under Ice and On the Seafloor	https://ntrl.ntis.gov/NTRL/

Sources: a) BSEE (2019), b) DOI [2021], c) National Technical Information Service (2021)

CITATION

McCourt J., C. McNeil, A. Marburg, D. Dickins, N. Michel-Hart. 2025. Detecting Oil Under Ice and On the Seafloor. U.S. Department of the Interior, Bureau of Safety and Environmental Enforcement. Report No.: 1155. Contract No: 140E0122C0008.

ABOUT THE COVER

Left photo by James McCourt/SL Ross Environmental Research showing evening tests at CRREL with oil targets illuminated from underwater by sensor package floodlights. Right photo by Applied Research Associates (ARA) showing deployment of sensor payload on Remus AUV at Ohmsett.

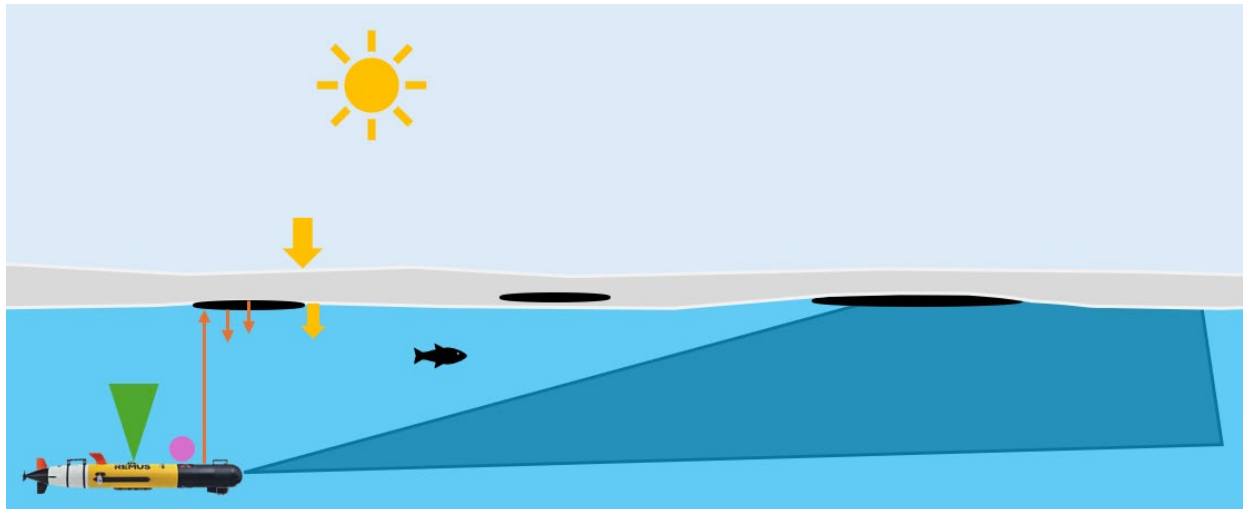
ACKNOWLEDGEMENTS

The authors would like to acknowledge the assistance of the following people, who made significant contributions to the successful completion of the project: Kathryn Trubac of the U.S. Army Corps of Engineers at CRREL, Alan Guarino, Grant Coolbaugh, and Anthony Logothetis

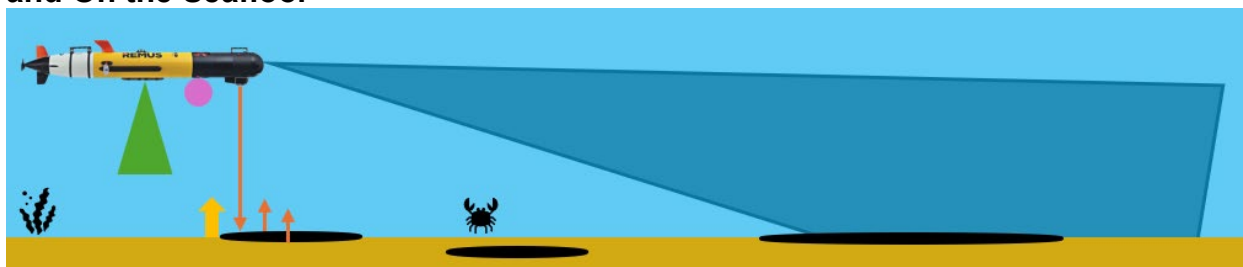
of Applied Research Associates at Ohmsett, and Chris Bassett and Andrey Shcherbina of the University of Washington, Applied Physics Laboratory

GRAPHICAL ABSTRACT

Detection of Oil Under Ice



and On the Seafloor



- Detects signal reflections from oil and ice or bottom
- 30 m range

Echosounder



- Detects oil from difference in reflectivity
- 100 m range

Imaging Sonar



- Detects BTEX or PAHs by fluorescence
- Range is immediate surrounding water

UV Fluorometer



- Detects oil by reduction in light intensity (direct or reflected)
- Range varies with depth and turbidity

PAR



- Detects oil by difference in appearance from surroundings
- Range varies with depth and turbidity

Camera



EXECUTIVE SUMMARY

There are several sensors that can remotely detect floating oil spills, but oil that is trapped beneath ice or has sunk to the seafloor is more difficult to locate. Most above-surface sensors (e.g., visual, infra-red, radar) perform poorly, are limited to a narrow ice temperature range, or do not work through water or ice. Researchers have tested different subsurface sensors and found performance varied depending on the spill circumstances; no sensor was the best for all conditions and a combination of sensors was recommended. The goal of this project was to develop an integrated system of sensors with different operating principles that could be installed on a suitable underwater platform and used to locate spilled oil that was either trapped under ice or had sunk to the bottom of the water body. While these would typically be two separate spill scenarios, previous research indicates that the same sensors should be useful in both circumstances (Hansen, 2009; Wilkinson 2015).

Published studies were reviewed to identify the most promising sensor operating principles and the best commercially available models. The selected sensors were tested on underwater vehicles looking upwards at oil under sea ice at CRREL, and downwards at submerged oil on the bottom of the water body at Ohmsett. The imaging sonar was able to identify submerged oil deposits, but pooled oil under ice did not appear significantly different from the surroundings. The echosounder was able to discriminate between pooled oil and ice when the oil was thicker than approximately 1 cm, but submerged oil on sand was not as distinct. The monochrome camera provided clear images of the oil deposits in both tanks. The photosynthetically active radiation sensor could detect pooled oil under ice and submerged oil on sand based on the significantly reduced light transmission. The UV fluorometer measured slight increases in oil concentration after oil was dispensed under ice, and near the submerged oil samples, but it was difficult to differentiate from normal background concentrations in the tanks.

Evaluating the sensor package in test basins was a necessary and important step in developing a remote system that could be deployed at a spill. However, there are significant differences between conditions at CRREL and Ohmsett, and what is expected at a real spill that would affect the performance of the sensors. A field trial in a natural environment is an important next step in developing and proving the sensor package.

GLOSSARY OF TERMS

ABS	Acoustic Backscatter
ADCP	Acoustic Doppler Current Profiler
AUV	Autonomous Underwater Vehicle
BSEE	Bureau of Safety and Environmental Enforcement
CDOM	Colored dissolved organic matter
CRREL	Cold Regions Research and Engineering Laboratory
CTD	Conductivity, temperature and depth
DO	Dissolved oxygen
GPR	Ground-penetrating radar
HDR	High dynamic range
HOOPS	Hoover Offshore Oil Pipeline System, a light crude from the Diana Hoover oil and gas field in the Gulf of Mexico
IR	Infrared
ISB	In-situ burning
LOD	Limit of detection
MP	Megapixel
OD	Outer diameter
PAR	Photosynthetically Active Radiation
ROV	Remotely Operated Vehicle
S/N	Signal-to-noise ratio
SSD	Solid-state drive
UV	Ultraviolet
UW/APL	University of Washington, Applied Physics Laboratory

Contents

List of Figures	viii
List of Tables	ix
1 Introduction	10
1.1 Oil Under Ice	10
1.2 Submerged Oil	12
1.3 Underwater Vehicles	13
1.4 Study Approach	14
1.5 Project Team	15
2 Sensor Selection	16
2.1 Sensor Development and Testing	16
2.1.1 Oil Under Ice	16
2.1.2 Submerged Oil	17
2.2 Sensor Technologies	18
2.2.1 Sonar	18
2.2.2 Optical	19
2.2.3 Fluorescence	21
2.3 Sensor Payload	21
3 Oil Under Ice Tests	23
3.1 Facility and Equipment	23
3.1.1 Ice Sheet and Test Areas	23
3.1.2 Oil Pools	24
3.1.3 Underwater Sensor Platform	26
3.2 Test Parameters	26
3.2.1 Sled Movement	27
3.2.2 Sensor Configurations	28
3.3 Observations	28
3.3.1 Weather and Ice Conditions	28
3.3.2 Test Areas	29
3.3.3 Oil Encapsulation	29
3.4 Sensor Results	31
3.4.1 Imaging Sonar	31
3.4.2 Echosounder	32
3.4.3 Camera	35
3.4.4 PAR	37
3.4.5 UV Fluorometer	40
4 Submerged Oil Tests	41

4.1	Facility and Equipment.....	41
4.1.1	Test Oils.....	41
4.1.2	Submerged Oil Targets.....	41
4.1.3	Underwater Platforms	44
4.2	Test Parameters	45
4.3	Observations.....	46
4.3.1	Weather Conditions	46
4.3.2	Remus 100 AUV Operation	46
4.4	Sensor Results.....	47
4.4.1	Imaging Sonar	47
4.4.2	Echosounder.....	49
4.4.3	Camera	53
4.4.4	PAR	54
4.4.5	UV Fluorometer	55
5	Conclusions.....	59
6	Recommendations	61
6.1	Field Trial Design Considerations	62
7	References.....	63
	Appendices	66

List of Figures

Figure 1: Block diagram for sensor payload	22
Figure 2: CRREL Geophysical Research Facility	24
Figure 3: CRREL test layout.....	24
Figure 4: Drilling hole through ice sheet.....	25
Figure 5: Delivering oil to Test Area 5	25
Figure 6: Wheeled cart with sensor payload	27
Figure 7: Pulling lines	27
Figure 8: Electric winch	27
Figure 9: Test areas on Friday, February 9	30
Figure 10: Test areas on Thursday, February 15	30
Figure 11: Identifiable features below ice sheet from imaging sonar.....	31
Figure 12: Echogram as Test Area 6 was filled with oil	33
Figure 13: Echogram as Test Area 4 was filled with oil	33
Figure 14: Echogram collected as the sensors moved across the tank.....	34
Figure 15: Echogram corrected for depth using pressure sensor data.....	35
Figure 16: Test areas viewed from below with the monochrome camera.....	36
Figure 17: Test areas at night, illuminated by SeaLite LED floodlights	36
Figure 18: Test areas illuminated from beneath the ice with Sealite LED floodlights	37
Figure 19: PAR measurements from beneath ice over 48 hours.....	38
Figure 20: PAR measurements as sensor moved across tank.....	39
Figure 21: PAR data analyzed to identify minimum values corresponding to oil pools..	39
Figure 22: UV Fluorometer measurements before and after oil was distributed.....	40
Figure 23: Pans filled with sand and cement mixture	42
Figure 24: Pans with visual markers and test oils	44
Figure 25: Submerged oil pan layout at Ohmsett	44
Figure 26: Underwater platforms used at Ohmsett.....	45
Figure 27: Images from BlueView sonar at Ohmsett.....	48
Figure 28: Analysis of BlueView Imaging Sonar results for submerged oil detection	48
Figure 29: Automatic detection algorithm results for Test Pan 12 varying S/N ratio.....	49
Figure 30: Echogram as Raven ROV hovered over Test Pan 7	50
Figure 31: Echogram as Raven ROV hovered over Test Pan 10	50
Figure 32: Echogram as Raven ROV hovered over Test Pan 12	51
Figure 33: Compiled echograms from Raven ROV transit	52
Figure 34: Echogram as Raven ROV passed through dispersed oil plume.....	53
Figure 35: Monochrome camera images of selected test pans	54
Figure 36: Nighttime operation of Raven ROV with LED floodlights.....	54
Figure 37: PAR measurements from Raven ROV pass over test pans	55
Figure 38: PAR measurements from Mission 8 transit of Raven ROV	56
Figure 39: UV Fluorescence measurements from Remus 100 AUV	57
Figure 40: Raven ROV traversing dispersed oil plume.....	58
Figure 41: UV Fluorescence measurements of dispersed oil plume	58

List of Tables

Table 1: Overview of some spill scenarios that could lead to oil under ice.....	11
Table 2: Potential submerged oil spill scenarios	13
Table 3: Promising underwater sensor technologies for detecting oil under ice.....	17
Table 4: Selected acoustic sensors.....	19
Table 5: Selected optical sensors	20
Table 6: Selected fluorescence sensor	21
Table 7: Sequential filling of Test Area 6.....	25
Table 8: Oil amounts and measured slick dimensions	26
Table 9: Weather conditions during testing at CRREL	29
Table 10: Oils used in submerged oil tests.....	42
Table 11: Test pan contents and appearance	43
Table 12: Weather conditions during testing at Ohmsett.....	46
Table 13: Qualitative performance of sensors to detect oil.....	60
Table 14: Field trial research questions.....	61

1 Introduction

A significant concern about oil spills in remote Arctic regions, whether they originate from oil exploration and production, subsea pipelines, oil tankers, shore facilities, or other vessel traffic, has been the possibility that oil could become trapped under ice where it is out of sight, making it difficult to find and recover. While there are multiple platforms and sensors such as vessels, aircraft, and satellites, that can remotely detect floating oil spills (Leifer et al., 2012), finding oil spilled in the presence of ice is significantly more challenging. Depending on factors such as the source of the spill, the time of year, and length of time since the spill occurred, oil may be on top of the ice (and possibly covered in snow), on the water between ice floes, under the ice, or encapsulated within the ice (Owens and Dickins, 2015). Most above-surface sensors perform poorly in these conditions. Past studies and recent work using ground-penetrating radar and trained dogs have shown potential to detect oil under ice and snow, but these techniques require a stable ice surface to work from safely (Bradford et al. 2010 & 2015; IISD, 2025 – in preparation).

A similar challenge is posed by oil spills that sink to the bottom of a water body, as may occur from spills of heavy oil aggregated with sand or sediment, or some in-situ burn residues. Most above-surface sensors do not work through deep water, but subsurface sensors have shown promise (Hansen et al. 2009).

Underwater platforms can operate under a wide range of conditions and subsurface sensors have shown promise at detecting oil under ice (Wilkinson et al., 2015). In a multi-sensor test conducted in the CRREL controlled climate basin in 2015, researchers concluded that no single sensor type can detect oil under all conditions, and that the best chance of success is to use multiple sensor types that can expand the operating envelope (Pegau et al., 2016). However, a complete system that could be deployed at a spill has not yet been developed and proven. The goal of this project was to develop a self-contained package of several complementary sensors that could be installed on a suitable underwater platform and used operationally at a spill to find oil under ice or submerged oil.

1.1 Oil Under Ice

While oil spills in the Arctic are rare (NASEM, 2022), there is still a chance of a significant spill becoming trapped under ice. Potential sources include ongoing oil production and exploration activities in Cook Inlet and the Beaufort Barents, Pechora and Kara Seas, and vessel traffic through Arctic regions, which has increased with recent decreases in the extent, duration and severity of sea ice. Geopolitical tensions have spurred interest by shipping companies to find safer and shorter routes. Examples of these global influences serving to increase Arctic spill risks include rebel attacks on shipping in the Red Sea, and Russian efforts to circumvent sanctions on tankers moving domestic crude oil to market. The latter has led to the recent use of low-ice class, aged tankers and cargo vessels to transit the Northern Sea Route through the Bering Strait. There is also a risk from pipelines or rail lines near freshwater lakes and rivers in cold regions, such as the Great Lakes. Table 1 presents a summary of potential spill scenarios that could lead to oil under ice, and some of the challenges to detecting the oil.

Table 1: Overview of some spill scenarios that could lead to oil under ice

Possible Spill Source	Typical Oil Types	Challenges to Detection
Exploration and Production Activities (e.g., drilling rigs, pipelines)	Crude oil, condensate	New ice growth can encapsulate the oil
Vessels transiting Arctic or sub-Arctic ice-covered areas	Marine diesel Fuel oils (IFO 180 to 380, low-sulfur fuel oils) Crude oil Heavy bunker oil	Ice varies greatly in thickness with roughness features that can obscure the appearance and detection of trapped oil
Pipelines near freshwater and marine coastlines	Conventional and non-conventional (e.g., dilbit, synthetic crude) crude oils Condensate	

Oil production activities in the U.S. Outer Continental Shelf that could result in spilled oil under ice are confined to the Alaska region. Potential spill sources in this region include possible future offshore exploration wells from floating drilling units in the Chukchi or Beaufort offshore areas (no current activity), and marine pipelines in shallow water (e.g., existing out to ~12 m depth at Northstar Island, and possible future pipelines connecting to the proposed Liberty field). Spills from existing and proposed production facilities on artificial and natural islands off the North Slope, specifically Northstar, Ooguruk, and Nikaitchuq and, and the proposed Liberty development, could lead to substantial volumes of oil on ice (e.g., from a surface blowout) but less likely under ice.

The nature of the spill event (e.g., instantaneous or continuous release, surface or subsurface source, oil type, and prevailing temperature) will affect how the oil is distributed under the ice. In general, the expected behavior (Owens and Dickins, 2015; Dickins, 2011) should be as follows:

1. The roughness of the underside of the ice surface can contain large quantities of oil in a relatively small area. For example, analysis done for the Northstar development estimated that a 1,600 m³ spill would be contained under smooth, stable ice in an area less than 300 m in diameter (Dickins and Buist, 1999).
2. Oil trapped under ice will remain in a fresh, un-weathered state until it can surface in the spring. Unlike spills in open water, oil spilled under ice will not emulsify or disperse into the water column.
3. Oil will remain trapped under the ice, even in moderate currents. Currents in the order of 15-20 cm/s are needed to induce oil movement, while typical winter currents under the ice in the Beaufort Sea are on the order of 5 cm/s or less. More viscous oil under rougher ice could require much higher current velocities to move under a static ice cover.
4. Offshore, oil trapped beneath moving pack ice will drift with the ice.
5. Instantaneous (aka “batch”) spills that occur early in the season are likely to become encapsulated in the ice. For example, oil deposited under ice in a batch release from a pipeline rupture could become encapsulated with new ice growing beneath the oil in 24 to 72 hours depending on air temperatures and ice thickness at the time of the spill.

6. Oil being continually replenished, such as in the case of an uncapped subsea blowout under ice from a late season exploration blowout, may remain under the ice for as long as the well continues to flow and the ice remains closely packed.

The possible occurrence of distinct trapped oil layers under sea ice off the North Slope is a seasonal problem, stretching from November when landfast ice exceeds the minimum thickness to avoid rapid surfacing (~25 cm), until May when any oil spilled under ice will rapidly migrate to the surface through the warming, porous ice sheet. Responders would have to wait until December in most years for the ice to become stable and thick enough to safely support on-ice operations at any significant distance from shore.

1.2 Submerged Oil

A review of incidents involving sunken oil (API, 2016) determined that oil may sink under the following circumstances:

- Heavy refined products (e.g., residual fuel oil, coal tar, or slurry oil) that are denser than water can sink immediately.
- Some heavy crude oils and diluted bitumen products may float initially but sink after weathering.
- In areas with high suspended solids concentrations, oil may form oil-particle aggregates that are denser than water and sink.
- Weathered oil may mix with sand and sediment on shorelines to form mats that are denser than water and sink.

Sinking may occur more frequently in fresh water and brackish water systems because the density difference between the oil and the water is reduced, compared to oil spilled in a marine (salt laden) environment. In all cases, the sunken oil can become mixed with or buried by sediments, which may further complicate detection efforts.

In situ burning can produce residues that sink after they cool (Buist et al., 1997), and there may only be a short window of opportunity to collect the residue on the surface following a burn before it cools and sinks. During the Deepwater Horizon Response, over 400 in situ burns were conducted and most produced residue that sank (Shigenaka et al., 2017). While in situ burning generally results in a net environmental benefit, sunken residues may foul fishing nets or result in localized benthic impacts, hence the value in identifying and locating sunken oil, and monitoring any movement over time. Table 2 presents a summary of possible submerged oil scenarios that were considered, and some of the challenges to detecting the oil.

Considering the Outer Continental Shelf Region, Arctic submerged oil scenarios are much less likely and much more specific to the circumstances of the incident. All crude oils currently produced off the North Slope have sufficient buoyancy to quickly rise through the water column in the winter months and potentially be trapped under ice. The heaviest crude produced in Alaska at present is from Milne point – 20-21 API gravity or ~0.93 specific gravity. Even this oil will float in seawater when fresh.

Table 2: Potential submerged oil spill scenarios

Possible Spill Source	Typical Oil Types	Challenges to Detection
In-situ burning	Burn residue	Reduced visibility due to depth and possible turbidity
Transportation Infrastructure (e.g., pipelines, rail cars, barges)	Refined heavy oils Weathered diluted bitumen and similar	Lack of contrast with bottom if oil is mixed or coated with sediment
Oil-Particle Aggregates and Mats	Weathered Crude oil Medium to heavy fuel oils Diluted bitumen and similar	

In order for traditional crude oils to sink and be deposited on the seabed, they would need to be exposed to extensive weathering, incorporate considerable amounts of sediment (e.g., off the Colville Delta), or be modified to become denser through in-situ burning (ISB). In either case, the sinking would likely take place during the open water period or during break-up: for example, in response to a summer spill from a North Slope production facility or pipeline, that drifts into sediment laden waters or is subject to ISB with firebooms in open water.

In the winter, surface blowouts at a production facility could deposit large volumes (thousands of m³) on the ice surface around an artificial island. If the heavily oiled snow is subsequently burned, the unrecovered residue could potentially sink to the seabed during ice break-up in July. Oil on the seabed could also result from an exploration well blowout where considerable bottom sediments are entrained in the oil exiting from the well bore, as was observed close to the discharge point in the Deepwater Horizon spill.

1.3 Underwater Vehicles

Advancements in battery and micro-processor technologies over the past decade have significantly improved the capabilities of underwater robotic platforms. These vehicles can be divided into two categories based on how they are operated:

- Remotely Operated Vehicles (ROVs) are connected to an operator via a tether that supplies power and communications for operational control and data sensors. This configuration allows the remote operation of the platform up to the practical limits of the cabling.
- Autonomous Underwater Vehicles (AUVs) are powered by internal batteries and must be pre-programmed to follow a defined route or rely on sensors to assist in navigation. Once deployed, an AUV will complete its mission and travel to a pre-programmed location where it can be retrieved, and data downloaded.

Both platforms can be fitted with a range of cameras, lights, and a multitude of additional sensors. A ROV could be used for spills where the survey area is limited, and may be easier to operate in an area with obstructions, such as around a production platform. AUVs have a

significantly longer range and would be better able to survey larger areas or operate in deep water but have limited on-board power that can restrict range and payload.

1.4 Study Approach

The goal of the project was to prototype a self-contained system of sensors that could be installed on suitable underwater vehicles and used to detect spilled oil that has been trapped under ice or submerged at the bottom of a water body. Requirements for the system included:

- The sensor package should function on a variety of relatively small autonomous and remotely operated underwater vehicles (e.g., portable by a two-person team) capable of deployment at spills in remote areas, a requirement that imposes power and size limitations.
- The system should function in a variety of environmental conditions, including cold water close to freezing with ice, fresh and salt water, and in both shallow and deep water (up to about 100 m).
- There should be a mix of sensors that can interrogate targets close to the vehicle (< 3 m) and further away (~ 30 m).
- The sensors should be configured to detect both oil under ice and submerged oil (i.e., upward and downward looking), despite the significant differences in the types of oil and presentations between the two scenarios.
- The sensors must be integrated as part of a remotely operated or autonomous underwater platform capable of navigating from their point of deployment to the spill site and back.

No such system has been developed, and it was understood from the outset that significant research would be needed to reach the prototype stage. Oil spill detection is not a primary market for sensor manufacturers, and some adaptations and modifications were expected to successfully apply individual sensors in these new applications. With that in mind, it was felt that focusing on modifying proven and mature, off-the-shelf sensors offered a better chance of success than trying to develop more experimental technologies.

The project was completed in several stages, as follows:

1. Previous research on underwater remote oil sensing was reviewed to identify promising detection techniques.
2. The most suitable models of commercially available sensors were identified and purchased.
3. A pressure-housing to mount, power, and operate the sensors was designed and fabricated.
4. The sensor package was mounted on a ROV and an AUV and tested in tanks under controlled conditions with oil under ice and submerged oil targets.
5. The data from individual sensors was analyzed to identify signatures indicating oil, and a methodology to streamline the analysis and combine data streams from multiple sensors was developed.
6. A field trial was outlined to address scale-issues that prevented the full assessment of the capabilities of the sensor package in test basins.

To-date, operational subsurface detection systems have tended to be much larger and/or more expensive, have limited sensor types and primarily designed to look upwards. This project builds

on previous research while focusing on developing a nimbler multi-platform sensor suite that can be deployed beneath ice (or in open water) to look at oil targets upwards and downwards.

1.5 Project Team

The project team brings a combined engineering and science approach:

- The project lead was SL Ross Environmental Research Ltd., which has over 40 years of experience in oil spill research and response, with many projects addressing Arctic spills
- University of Washington Applied Physics Laboratory brings unparalleled expertise in sensors and data processing with ROVs and AUVs in Arctic field deployments.
- DF Dickins Associates LLC has over 50 years of environmental engineering experience in Arctic Environments and Remote Sensing.

2 Sensor Selection

The project goal was to develop a package of sensors and controlling software that can detect spilled oil in the following two scenarios: i) floating oil that has become trapped under or within an ice layer, and ii) sunken oil that is located at the bottom of a water body. These two general spill conditions have implications regarding the spill origin and types of oil that would tend to be involved, and present inherent challenges to detecting the oil.

2.1 Sensor Development and Testing

The project team reviewed previous research on remote detection to identify the most promising operational principles.

2.1.1 Oil Under Ice

Much of the early research on spill detection in ice took place over a ten-year period beginning in the late 1970s, motivated by offshore drilling programs in the Canadian Beaufort Sea, and exploration and production off the North Slope of Alaska and in Cook Inlet. Researchers carried out analytical, bench, and basin tests and field trials using a wide range of sensor types: acoustics, radar, ultraviolet fluorescence, infrared (IR), gamma ray, microwave radiometer, resonance scattering theory, gas sniffers, and ground penetrating radar (GPR) (Dickins, 2000).

Fingas and Brown (2017) reviewed the state of the art in specialized remote sensing technologies for oil spill detection in open water and ice, while Leifer et al. (2012) provided a review of satellite and airborne systems and sensors based on their performance in the open water Deepwater Horizon response.

Our present knowledge of which sensors are most likely to succeed in different oil-in-ice scenarios is based largely on experiences with temperate spills supported by a small number of field tests and tank/basin experiments with deliberate spills on and under ice. In 2004 and 2006 the US Minerals Management Service (now BSEE) and industry funded several test basin studies at the US Army Corps of Engineers Cold Regions Research and Engineering Laboratory (CRREL) as well as a field release of crude oil under ice on Svalbard, Norway, to evaluate the capabilities of ground penetrating radar (GPR) and methane gas “sniffers” to detect oil in and under ice (Dickins et al., 2005 and 2006; Bradford et al., 2010 and 2015). Subsequent testing in the CRREL outdoor basin showed that underwater acoustic sensors (sonar) could effectively detect oil layers under ice (Wilkinson et al., 2015).

The SINTEF Oil in Ice Joint Industry Project evaluated a range of sensors looking at oil spilled in offshore pack ice in the Norwegian Barents Sea in 2008 and 2009 (Dickins et al., 2010). The Arctic Response Technology JIP (2012-2017) assessed the state of knowledge in both surface and subsurface sensor technologies. Following this assessment, in 2016, the JIP commissioned the Prince William Sound Oil Spill Research Institute (OSRI) to lead a team of specialists in evaluating the capabilities of different remote sensing technologies in detecting and mapping oil in and under ice at CRREL (Pegau et al., 2016). This unique program represented the first deployment of an array of above-surface and subsea sensors under controlled conditions with simultaneous multi-sensor data. A series of oil releases spanned an entire ice growth cycle from

initial freeze-up to the final melt. Key findings were that three underwater sensor technologies were likely candidates for successful development into operational systems, as summarized in Table 3.

Table 3: Promising underwater sensor technologies for detecting oil under ice

Sensor	Operating Principle	Limitations
Visible/Optical (Cameras recording still images or video.)	Detects oil based on difference in appearance from background.	Required daylight or light source to illuminate or back-light oil layer, which will be reduced as ice or snow thickness increase. Can provide indication of extent of oil, but not thickness.
Acoustic/Sonar (e.g., multi-beam, broadband, narrowband, single beam, echosounders)	Acoustic sensors operate by transmitting sound pulses (sometimes called pings or chirps) and measuring the strength of the return pulses. The difference in strength between the transmitted and reflected signals depends on the resistance of the medium to sound transmission (acoustic impedance), which depends on the material (e.g., ice, oil, sediment). Analysis of the return signals can determine the presence and possibly thickness of an oil layer.	Acoustic frequency affects the scale of features that can be resolved, including oil layer thickness. Frequency can be selected with some models. Beam width and shape will vary.
Laser-induced Fluorescence.	A laser excites aromatic molecules in oil that fluoresce at a different light wavelength from the laser. Detecting the return signal positively identifies the presence of hydrocarbons.	Some naturally occurring materials fluoresce at similar frequencies, which can result in false positives; polarization can help to reduce these.

Recommendations were based on the likely potential of a sensor to detect and/or measure the presence/thickness of fresh crude oil spilled under sea ice with up to 6 cm of new ice growth beneath the oil. Under the scenario of encapsulated oil layers trapped with more than ~6 cm of new ice growth beneath the oil, only two sensor types, low light level cameras and sonar, showed any substantive potential.

2.1.2 Submerged Oil

Spills involving submerged oil are rare, but cleanup has historically been challenging, time-consuming, and expensive. Locating submerged oil deposits after spills has often required laborious reviews of currents and geomorphology to identify quiescent areas where oil might collect, followed by direct sampling or manual reconnaissance (e.g., Enbridge, 2021; Dollhopf et al., 2014).

Tests conducted at Ohmsett by the US Coast Guard (Hansen et al., 2009) evaluated the ability of four systems to locate and identify (differentiate) test patches of heavy oil on the bottom of the tank:

- Multi-beam sonar (RESON Inc. SeaBat 7125)
- Laser-induced fluorescence (SAIC Laser Line Scan System)
- Fluorescence polarization (EIC Laboratories FP)
- In-situ fluorometer and mass spectrometer (Woods Hole Detection and Identification System)

The study reached similar conclusions to those made by the Arctic Response Technology JIP: the sonar and laser-induced fluorescence polarization sensors showed the most promise.

2.2 Sensor Technologies

Previous studies showed that no single sensor type was best for all conditions, and multiple sensor types operating together were recommended (Pegau et al., 2016). The most promising sensor types were based on i) sonar, ii) optical, and iii) fluorescence principles. The project team reviewed commercially available technologies to inform the selection of the best devices for each mode for use on underwater platforms.

2.2.1 Sonar

Acoustics have been used to detect and identify objects in the water for nearly a century, and commercial products of varying capabilities are widely available. These devices operate by generating a relatively short sound pulse and receiving the echo reflected off surfaces. This technique was initially used for measuring water depth and has since been adopted for a broad range of applications. By analyzing differences in the sound pulses reflected by ice, the bottom, and oil layers, it is possible to differentiate between them. The principles that make oil detection using sonars possible are well-established, despite the relative novelty of the application.

Commercially available instruments operate over a range of frequencies from single kHz to greater than 1 MHz and are available in numerous geometries that span from imaging of wide swaths of the water column to focused, narrow beams. Systems can be separated into two categories, as follows:

- Echosounders, which typically rely on a single transducer to transmit and receive signals, and interrogate a cone-shaped area of the water with a narrow beam width (e.g., 20° or less)
- Imaging systems, which use more complex arrays of receivers to allow scanning of larger swaths of the water (e.g., 100° or more)

Our review determined that the best combination of acoustic sensors was i) an imaging sonar capable of surveying a wide area in a relatively short amount of time, coupled with ii) an echosounder that could conduct quantitative analysis, such as measuring oil layer thickness. The models selected for the project are summarized in Table 4.

The BlueView M900 imaging sonar is a reliable product from one of the largest oceanographic supply companies in the world.

The Signature 1000 Acoustic Doppler Current Profiler (ADCP) has five beams that insonify a cone-shaped sampling volume out to maximally 30 m from the instrument. For this study conducted in quiescent waters, sampling focused on the ADCP's central fifth beam, which then

functioned like a high resolution echosounder. For missions conducted in real oil spill environments with significant flow fields, the ADCPs data collection firmware could be reconfigured to also measure currents using the other four beams. Multi-mode sampling could be accomplished by interleaving the different ping sequences in time with no impact on data quality.

Table 4: Selected acoustic sensors

Sensor Type	Make and Model	Specifications
Imaging Sonar	Teledyne Marine BlueView M900-130-S-MKS(W) sonar	Field of view 130° Range 100 m
Echosounder (ADCP)	Nortek Signature 1000 ADCP	Range 30 m Resolution 3 mm to 0.25 m Beam width 2.9°

A second echosounder operating at a lower frequency could be helpful in detecting oil encapsulated in ice, as lower frequency sound waves may penetrate deeper into ice. However, the frequency of the produced sound pulse is inversely proportional to the size of the transducer, and smaller sensors suitable for use on underwater platforms will necessarily use smaller transducers and operate at higher frequencies. A low-frequency device would be larger and heavier, and possibly more difficult to integrate on an AUV.

2.2.2 Optical

Optical detection techniques that were considered included using cameras to capture visible or near-visible images, and radiometers to measure light transmission. Light attenuation from depth, turbidity, and the thickness of the ice layer and snow cover will reduce the effectiveness of optical techniques. In general, they will be good at detecting the edges of oil pools (and thus oil extent), and in some cases may offer some information for estimating oil layer thickness.

Cameras were an obvious choice due to our natural fluency with visible imagery and the availability of high-resolution cameras. Cameras can detect oil if it appears sufficiently different from the surroundings, and image processing can automate the detection process. Cameras can also provide useful information about the surroundings and location of the underwater platform relative to the target.

Radiometers are devices that measure the intensity of electromagnetic radiation with far greater sensitivity, dynamic range, and precision than a camera. A variety of sensors have been developed using different wavelengths of radiation, depending on the application. Some of these could be used to detect oil by measuring differences in the amount of light that passes through oil layers compared to the surrounding ice or is reflected by oil layers compared to the surrounding bottom. The data from radiometers is simpler to process and analyze compared to images, which is advantageous for AUVs with their limited onboard resources. Multispectral radiometers provide wavelength dependent detection and may help differentiate between various causes of light variability under ice. Standard oceanographic wavelength filtered radiometers include the Photosynthetically Active Radiation (PAR) sensor designed to detect light suitable for phytoplankton growth.

The models of optical sensors selected for the project are summarized in Table 5.

Table 5: Selected optical sensors

Sensor Type	Make and Model	Specifications
Monochrome Camera	Lucid Vision PHX122S-MC-IX monochrome camera	Resolution 4024 x 3036, 12.2 MP Framerate 9.1 FPS
Color Camera	Lucid Vision TRI054S-CC color camera	Resolution 2880 x 1860, 5.4 MP Framerate 20.8 FPS
Photosynthetically Active Radiation Sensor	Biospherical Instruments Inc. MPS-PAR	Spectral range 400 to 700 nm LDL $2.5 \times 10^{-9} \mu\text{E}/\text{cm}^2\text{s}^2$

Initially, two cameras were considered, both Gigabit Ethernet machine vision cameras from Lucid Vision Labs (Richmond, BC). The two cameras differed primarily in the imaging sensor used, and once mounted in their waterproof housing were identical to integrate from a mechanical and software perspective. The monochrome camera uses a 12.2 MP Sony IMX226 sensor, a high-sensitivity sensor designed for low-light security and CCTV applications. The color camera uses the 5.4 MP Sony IMX490 sensor, which is designed for the automotive market and features a dual-sensor construction that allows the simultaneous capture of high-dynamic-range (HDR) imagery without post processing. Though lower resolution than the monochrome sensor, the IMX490 presented an opportunity to consider the utility of HDR imaging when observing dark oil patches against a very bright background.

The Biospherical MPS-PAR measures solar radiation between 400 and 700 nm, with a dynamic range of 10 orders of magnitude. With that level of sensitivity, it was hoped that the sensor would be able to differentiate between light attenuation caused by natural variations in ice thickness and snow cover, and the presence of trapped oil. It was unclear if the sensor would also be able to detect submerged oil based on differences in light reflected off the bottom and off submerged oil deposits.

Previous experience by the project team using PARs suggested that restricting the view angle of the sensor with a collimator could be beneficial. The larger the field of view of the PAR sensor the more light enters the sensor from different view angles, resulting in an effective spatial smoothing of the signals from the light reflected and scattered from the environment around the test sample. Higher spatial resolution should help identify relatively small oil targets based on differences in light transmission. The collimator would reduce signal intensity, but this was not expected to reduce performance because of the high dynamic range of the Biospherical MPS-PAR. Custom collimators were fabricated and used with the PAR sensors on each vehicle to ensure more directionality from the light gathering by the sensor.

Two LED floodlights (Deep Sea Power and Light LSL-2000 Sealites) were mounted on the payload system to provide additional illumination. The lights could be activated and dimmed remotely. As implemented, they operated continuously once turned on; however, a trigger or strobe function linked to the camera operation could be implemented to limit power consumption.

2.2.3 Fluorescence

Fluorescence sensors operate on the principle that aromatic molecules present in most oils are excited by light at certain frequencies (typically 300 to 400 nm) and fluoresce at different frequencies (400 to 600 nm, depending on the compounds present). There are some naturally occurring materials that fluoresce at similar frequencies to oil (e.g., chlorophyll at 614 nm) and can confound the results, but there are methods to screen these out (e.g., polarization). Fluorescence has been used in oil spill response for monitoring dispersant use and in other industries for leak detection, and commercially available instruments are available.

As with optical sensors, the transmission of light is strongly attenuated in water, and these devices have a very limited range and typically interrogate an area very close to the sensor. Unlike optical and sonar methods, fluorescence is theoretically able to positively confirm the presence of oil (as opposed to an anomaly that could be oil). Currents, depth profiles, intervening ice or sediment layers, and variable solubility of the target oils present significant challenges, but it was hoped that even a small increase above background concentrations around anomalies detected by the other sensor modes will be able to confirm the presence of oil. The model of fluorescence sensor selected for the project is presented in Table 6.

Table 6: Selected fluorescence sensor

Sensor Type	Make and Model	Specifications
UV Fluorometer	Chelsea Technologies Ltd. UviLux 2141-001-HB	Excitation 255 nm Sensitivity: <ul style="list-style-type: none">• 0.010 to 150 µg/L Phenanthrene

The UviLux is an in-situ digital fluorometer that can be configured to detect a variety of substances in the water column, including monocyclic aromatic hydrocarbons (including benzene, toluene, ethylbenzene, and xylene, often referred to as BTEX), and Polycyclic Aromatic Hydrocarbons (PAHs). The sensor purchased was configured to detect PAHs, as these are typically present in both light and heavy oils, and it was anticipated that one sensor would work for both oil under ice and submerged oil scenarios. Chelsea Technologies is one of the leading manufacturers of fluorometers and this model had a very high sensitivity that would be useful in detecting the expected low concentrations of target compounds.

One of the uncertainties with field use will be effects of oil contamination on the underwater platform or sensors – if oil contamination occurs the sensor might lose sensitivity to trace oil detection. A cleaning protocol between field missions would be prudent.

2.3 Sensor Payload

The sensors were mounted in a purpose-built 19-cm OD (7.5-in) aluminum pressure housing that was fabricated at the University of Washington Applied Physical Laboratory. The housing was designed so the sensor payload could be mounted on different underwater platforms; the size, weight, and power requirements were based on what the Remus AUV platform could provide (see Section 4.1.3). The housing contained an integrated single-board computer with SSD

storage drive that performed all sensor coordination and data recording for the system. Power and data were transmitted through a single uplink connection to the vehicle chassis. A schematic representation of the housing and integrated systems is shown in Figure 1.

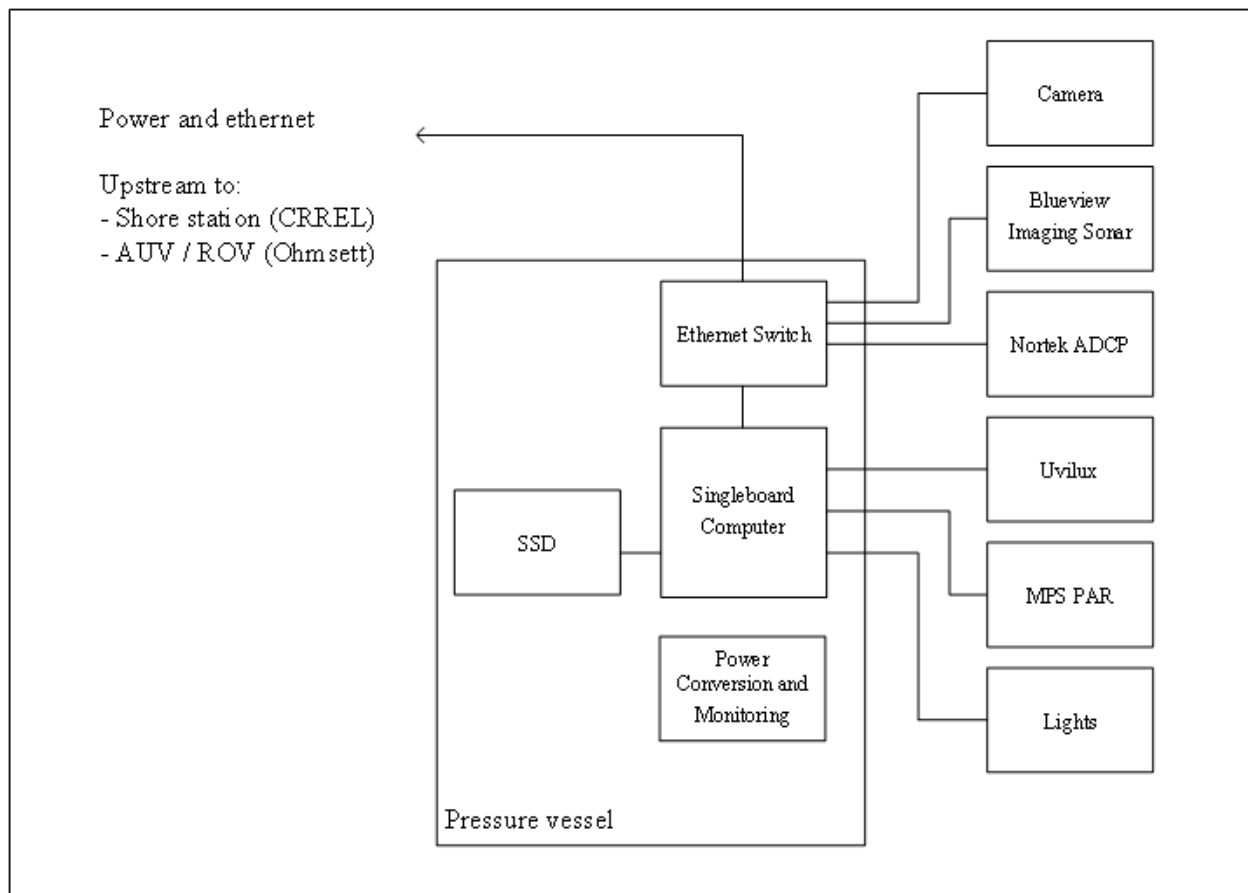


Figure 1: Block diagram for sensor payload

The payload configuration varied slightly between the basin tests at CRREL and Ohmsett (see Sections 3 and 4). At CRREL, the uplink connected to a 38-m (125-ft) tether providing 24 V nominal power and ethernet. Input voltage and current monitors were added to measure system power, due to the length of the tether and relatively low supply voltage. The sensors were remotely controlled from computers beside the tank, allowing real time data monitoring while the sensor payload was in the water.

At Ohmsett, on the Remus AUV, the sensor payload system connected to a port that provided power and ethernet, which was accessed through the Remus AUV management system. On the Raven ROV, the system connected to the data backbone of the vehicle, and sensors were monitored remotely over the Raven ROV tether.

3 Oil Under Ice Tests

The objective of the experiments was to evaluate the ability of the combined sensor package to identify and characterize oil targets that were located i) beneath an ice layer and ii) encapsulated within ice. The methodology was as follows:

- Grow a salt-water ice sheet and place oil pools of varying thickness underneath.
- Operate the sensors underwater
 - individually and simultaneously to evaluate effectiveness and possible interference, and
 - while stationary underneath oil targets and while moving across the tank.
- Allow the ice to grow and encapsulate the oil targets and then repeat the detection experiments.

The oil under ice tests were carried out between February 5 and 16, 2024.

3.1 Facility and Equipment

Several facilities were considered for testing under ice, including i) BSEE's Ohmsett facility in Leonardo, NJ, ii) the Large Ice tank at National Research Council (Canada) in St. John's, NL, and iii) the Geophysical Research Facility at the US Army Corps of Engineers Cold Regions Research and Engineering Laboratory (CRREL) in Hanover, NH. CRREL was chosen as the best location, despite the relatively small size of the tank, based on their ability to grow and maintain a sufficiently thick ice sheet, their willingness to deploy oil in their test basin, and their previous experience with similar experiments.

The CRREL Geophysical Research Facility (GRF) measures 18 m long, 7 m wide, and 2 m deep. The tank has a removable roof mounted on rails and is equipped with a refrigeration system that cools the water in the tank and the air above it. Subject to prevailing weather conditions, the tank can grow up to 2.5 cm of ice per day to a maximum thickness of approximately 50 cm.

3.1.1 Ice Sheet and Test Areas

CRREL started growing the ice sheet on December 8, 2023. Water salinity in the tank was representative of normal seawater, with a uniform salinity of $30\text{‰} \pm 0.2\text{‰}$. On January 22, 2024, CRREL staff cut six 1-m squares through the ice sheet, removed the ice in blocks, and let the sections refreeze to create areas with thinner ice and depressions that could contain oil (see Figure 2). Because the water in the test areas froze down from the surface and laterally from the edges, the depressions were dome shaped. On February 5, 2024, rectangular access holes were cut through the ice at each end of the tank to deploy and retrieve the sensor package. A schematic overview of the GRF layout is shown in Figure 3.

Ice cores were collected at various times to measure ice thickness and characterize the ice structure. On February 7, 2024, the ice sheet was 39 cm thick north and south of the test areas, and 49 cm thick in the middle; the ice over Test Area 1 (the control) was 28 cm thick. The thickness of the ice over the other Test Areas was measured on March 4, 2024, and ranged from 23 to 28 cm. Data from the ice cores is presented in Appendix B.



Figure 2: CRREL Geophysical Research Facility



Figure 3: CRREL test layout

3.1.2 Oil Pools

The oil used in the experiments was fresh Alaska North Slope crude oil (ANS), which had a density of 0.871 g/cm^3 . Oil was measured by weight into 20-L plastic containers and then delivered to the test areas using an electric peristaltic pump. A 15-cm diameter hole was drilled through the ice immediately to the east of each test area (Figure 4) and the tubing from the pump

was inserted through the ice to extend below the test area (Figure 5). Care was taken to fill the tubing with water before pumping oil to minimize introducing air bubbles beneath the ice sheet, as air bubbles are highly reflective to sound waves and could interfere with acoustic oil detection. Numbered tags were inserted through the ice beside each Test Area to help determine sensor position relative to the oil pools.



Figure 4: Drilling hole through ice sheet

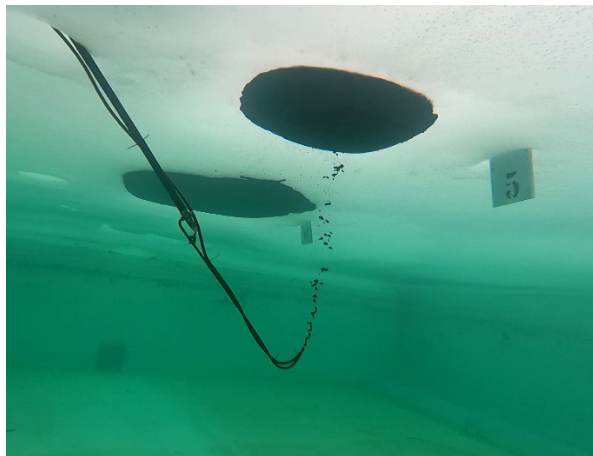


Figure 5: Delivering oil to Test Area 5

The oil pools in the test areas were intended to vary in thickness, with Test Area 1 having no oil and serving as the control and Test Area 6 having the most oil. The dimensions of the test areas could only be approximated based on the size of the cut areas and the overall thickness of the ice sheet because ice had grown in from all directions and not just the top down. For this reason, stepwise additions of oil were made first to Test Area 6 to determine the capacity. Oil was injected on February 8 in four stages, as summarized in Table 7. The sensor sled was positioned underneath the test area during injection to monitor the oil pool and gather data as the thickness of the oil layer increased. Based on this exercise, the maximum volume of each test area was approximately 60 L.

Table 7: Sequential filling of Test Area 6

Incremental Addition	Mass (kg)	Volume (L)	Total Volume (L)
1	4.37	5	5
2	4.36	5	10
3	17.4	20	30
4	26.1	30	60

Oil was injected into the remaining test areas on February 9. The amounts of oil distributed and the final slick dimensions are presented in Table 8. The sensor sled was moved below each test area as it was filled to record data while the oil was dispensed.

The area of the pools was determined by turning on the floodlights on the sled and measuring the length and width of the pools from the top of the ice sheet. The thickness of the middle of the oil

pools was measured on March 4, 2024, after operating the refrigeration system for several weeks to form ice beneath the oil pools and then measuring the heights of the cavities in the ice.

Table 8: Oil amounts and measured slick dimensions

Test Area	Mass (kg)	Volume (L)	Length (cm)	Width (cm)	Thickness (cm)
1	0	0	0	0	0
2	4.0	5	56	51	1.5
3	8.2	9	64	64	2
4	16.5	19	74	66	2.5
5	16.2	19	76	69	4
6	26.1	60	91	71	6.5

3.1.3 Underwater Sensor Platform

It was originally intended to mount the sensor package on a remotely-operated vehicle (ROV) for the oil under ice tests; however, the GRF tank was too shallow to maneuver a full-size ROV under its own power and there would not have been enough distance between the sensors and oil pools. The sensor payload was instead mounted on a custom-built, wheeled cart (Figure 6) that was pulled across the bottom of the tank at similar speeds to a ROV. The BlueView imaging sonar was mounted on the front of the sled; the angle of the sonar could be adjusted between horizontal and vertical. The Signature 1000 ADCP, MPS-PAR, UviLux fluorometer, and monochrome camera were on the top of the sled, facing up. Separate power and data cables were tethered to the rear of the cart and led to a control trailer beside the tank.

Line to pull the cart (Figure 7) was run through pulleys at each end of the tank. The lines were marked with distance to help determine the sled position and verify consistent start and end points. The cart was pulled manually across the tank for some tests, and for others was pulled faster using an electric winch (Power Hauler HD923EX, 200lb capacity, 2.3 hp, 90:1, Figure 8). The cart tracked straight when pulled southwards; however, it was observed to deviate approximately 10 cm from the center line when returned north to the starting point, likely due to the mass of the tether.

3.2 Test Parameters

In addition to the thickness of the oil pools, test variables included the speed the cart was pulled across the tank, individual sensor configurations, ambient conditions (e.g., light levels), and ice thickness under the oil slick. The permutations of tests from varying key sensor parameters and potential environmental and multi-sensor interferences was the basis for the test-matrix that was used throughout the experiment. The full list of test runs and equipment settings is provided in Appendix C.



Figure 6: Wheeled cart with sensor payload

1. Imaging sonar, 2. LED floodlights, 3. PAR, 4. UV Fluorometer, 5. Echosounder, and 6. Cameras



Figure 7: Pulling lines



Figure 8: Electric winch

3.2.1 Sled Movement

The speed of the cart across the tank was varied and included i) slow movement by hand-pulling and stopping for a short period (15 to 30 s) under each pad, ii) slow movement by hand-pulling without stopping, and iii) fast movement using the winch. The sensor payload did not include a direct measurement of cart speed. When pulled by hand, speeds were approximately 0.25 m/s. The winch operated at a constant speed, pulling the cart across the tank in 35 s, which is an average speed of 0.5 m/s. The cart position in the tank was determined by distance markings on the pulling lines and was also verified with the camera.

Cart speed did not affect sensor readings, except where increasing time of observation allows increased sensitivity (i.e., increased signal-to-noise ratio) by averaging across multiple readings. At high speeds, there is the possibility of inducing blurring in the camera, however the camera exposure time was capped at 1 ms to minimize blurring.

At the end of each run, the cart was pulled back to the north starting point by hand. The alignment of the cart was confirmed visually before each run and readjusted if necessary. The tethered cart allowed real time observation of sensor data, and monitoring of payload position to ensure sensors were centered on each oil patch. Real time monitoring also allowed adjustment of sensor parameters, although parameter modifications were minimized to ensure data remained comparable across the experiment.

3.2.2 Sensor Configurations

Each sensor has various settings that control operation, for example sampling rate and range. Depending on the sensor, several of the most important of these settings were varied to test their impact on oil detection. Runs were also completed with different sensors and possible environmental sources of signal noise turned off to assess the potential for interference. The BlueView imaging sonar was also tested with different orientations and lookout angles.

3.3 Observations

Observations made during the tests at CRREL are presented below.

3.3.1 Weather and Ice Conditions

In general, the first week of testing was unseasonably warm, with daytime highs from 9 to 12°C and overnight lows of 0°C. The ice softened later in the week and began to pull away from the edges of the tank by Friday, February 9; however, most of the oil remained contained beneath the ice sheet in the test areas and the warm weather did not impede testing. The weather was generally colder for the second week of testing and the ice firmed up. Starting on Thursday, February 8, the tank was covered with the roof each night to help maintain the ice sheet. Weather conditions during the test are summarized in Table 9.

Inspection of ice cores showed the skeletal layer (i.e., the soft bottom structure at the growing interface) was ~3 cm, which is thinner than would be experienced with thicker sea ice but not unusual at the thickness achieved in the tank. Photographs of an ice slab cut out of the unoiled ice on February 5 showed a distinct separation between milky ice in the upper part of the sheet and clear ice below. These layers commonly occur in natural sea ice and indicate zones with trapped air bubbles associated with relatively high growth rates early in the formation process. As the growth rate slows down, the air bubbles are expelled at the growing interface, resulting in much clearer ice.

Water temperature at the growing interface was in the range -1.3 to -1.6 °C indicating that new ice was not forming at the interface during the test period (the freezing point of water at 30 ppt is -1.8°C). The internal ice temperatures during the test period in the control core were close to isothermal, ranging from -1.8°C at the interface to -2.5°C near the surface at 8:45 AM. By the

afternoon, other cores taken in the unoiled ice showed upper ice temperatures as warm as -1.1°C , indicating that the ice was melting.

Table 9: Weather conditions during testing at CRREL

		Mon	Tues	Wed	Thurs	Fri	Sat	Sun
Week 1		Cloudy	Sunny	Sunny	Sunny	Cloudy	Sunny	P. Cloud
	Low ($^{\circ}\text{C}$)	4	-8	-10	-4	-3	0	-2
	High ($^{\circ}\text{C}$)	-1	3	3	7	8	13	6
Week 2		Overcast	Overcast	P. Cloud	Sunny			
	Low ($^{\circ}\text{C}$)	-2	-3	-9	-9			
	High ($^{\circ}\text{C}$)	5	2	-3	0			

Previous research where oil migration in natural sea ice was studied through an entire winter showed that a significant percentage of the oil spilled under the ice in mid-winter rose vertically to saturate much of the internal structure of the ice, eventually surfacing in late spring when the ice became close to isothermal (Dickins, 2011). The test site photographs shown below in 3.3.2 show evidence of this surfacing starting to happen. On this basis, the test ice created at CRREL in the GRF basin in 2024 is best viewed as representing sea ice during the melt phase, albeit much thinner than would typically be experienced, for example on the North Slope of Alaska at the end of the growth season (30 cm vs. 160 cm).

3.3.2 Test Areas

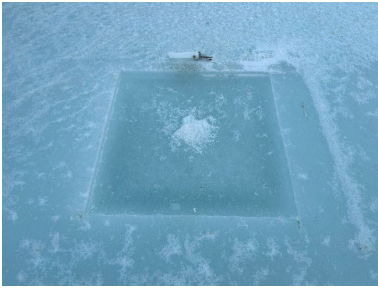
The appearance of the test areas from above the ice sheet on the afternoon of Friday, February 9 is shown in Figure 9. The oil pools were somewhat visible from above the ice sheet during daylight. Some surfacing of oil through the ice was noted above and to the North of Test Area 6 on Friday morning, and a small amount above Test Area 4.

The appearance of the test areas near the end of the tests on February 15 are shown in Figure 10. Additional surfacing of oil was noted in all test areas by the end of the two weeks, but the amounts were small enough to not significantly affect the experiment in terms of the oil layer thickness nor the expected response of the subsurface sensors. Generally, despite being unusually warm, the overall continuity of the ice sheet was excellent throughout the two weeks of testing.

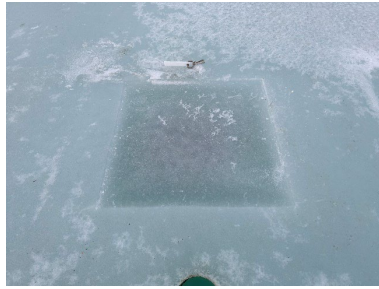
3.3.3 Oil Encapsulation

Starting on the morning of February 10, the cooling system was engaged continuously until February 13 to try to grow ice beneath the oil slicks in the test areas. Test runs were performed daily from February 13 to 15, and the cooling system was engaged immediately thereafter.

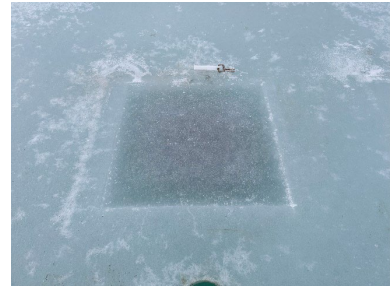
The oil slicks viewed underneath the ice with the monochrome camera appeared blurry compared to February 9, which indicated some ice growth had occurred. On February 15, an ice core was taken through Test Area 5 and a thin wire probe inserted through the oil slick to attempt to measure the thickness of the oil slick and strength of the underlying ice layer. A GoPro camera was inserted through the nearby access hole to observe the probe. The underlying ice layer was very thin with no strength to resist the probe, indicating that little oil encapsulation had occurred. This was a limitation of the cooling system in trying to compensate for warm air temperatures.



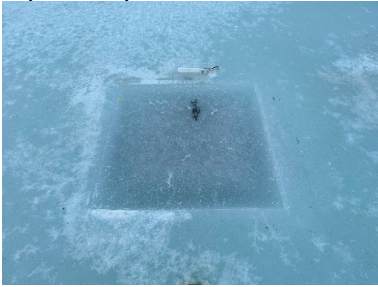
1 (control)



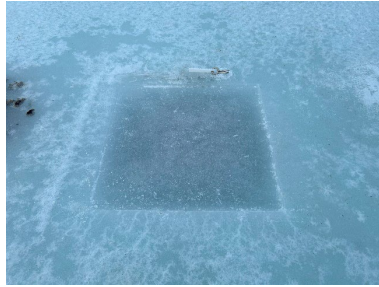
2



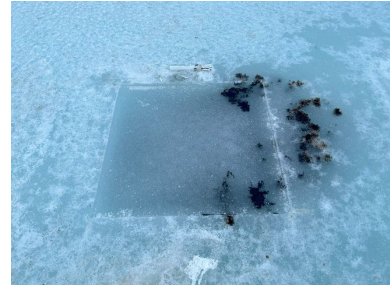
3



4



5



6 (thickest oil layer)

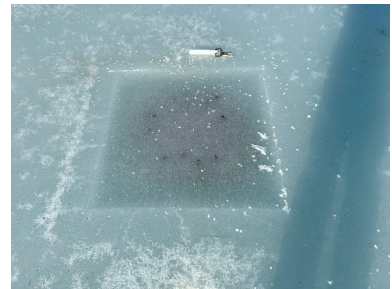
Figure 9: Test areas on Friday, February 9



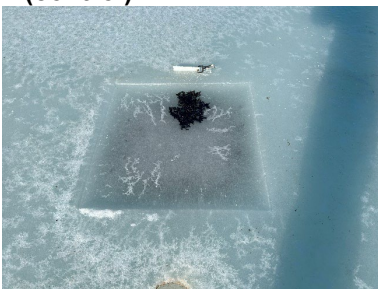
1 (control)



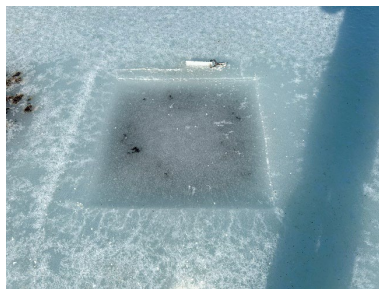
2



3



4



5



6 (thickest oil layer)

Figure 10: Test areas on Thursday, February 15

It was estimated that two or three more weeks of cooling would have been needed to generate significant ice growth (> 5 cm) beneath the oil slicks. Consequently, a further set of measurements were made on March 4 using the same wire probe technique to feel for top and

bottom of the oil cavity created by further new ice growth after completing the testing. These measurements are presented in Table 8, above.

3.4 Sensor Results

Observations and results from the sensors are discussed below.

3.4.1 Imaging Sonar

The native BlueView software that interfaces with the imaging sonar displays areas of high reflectivity (e.g., the walls of the tank and edges of the test areas) as bright, and areas of low reflectivity (e.g., the flat underside of ice, which does not reflect sound back towards the receiver) as dark. Similar to an optical camera, the BlueView imaging sonar measures shadow zones of low acoustic backscatter behind objects that strongly reflect the sound. Since the BlueView imaging sonar has multiple overlapping beams, there are additional fixed fan-shaped distortions where the beams merge, an artifact not found in conventional optical cameras even for wide-angle cameras (i.e., fisheye cameras which have other distortions of the image). Images from the sonar were viewable in real time as the cart moved across the tank and were also recorded on solid state drives for later processing and analysis.

The BlueView imaging sonar was oriented horizontally and interrogated a cone extending across the tank and up towards the underside of the ice. The sonar produced very clear acoustic images of the underside of the ice sheet (see Figure 11), particularly when moving; fine details such as the circular oil injection holes, and the sequentially numbered plates that extended through the ice beside each Test Area, were visible. Images when the cart was stationary appeared noisier and less detailed, as the reflected sound waves depend strongly on the angle of incidence and the geometry of the impacted surfaces, but this might also be perception since one's eye picks out persistent features more easily in a moving reference frame more than a stationary non-changing background.

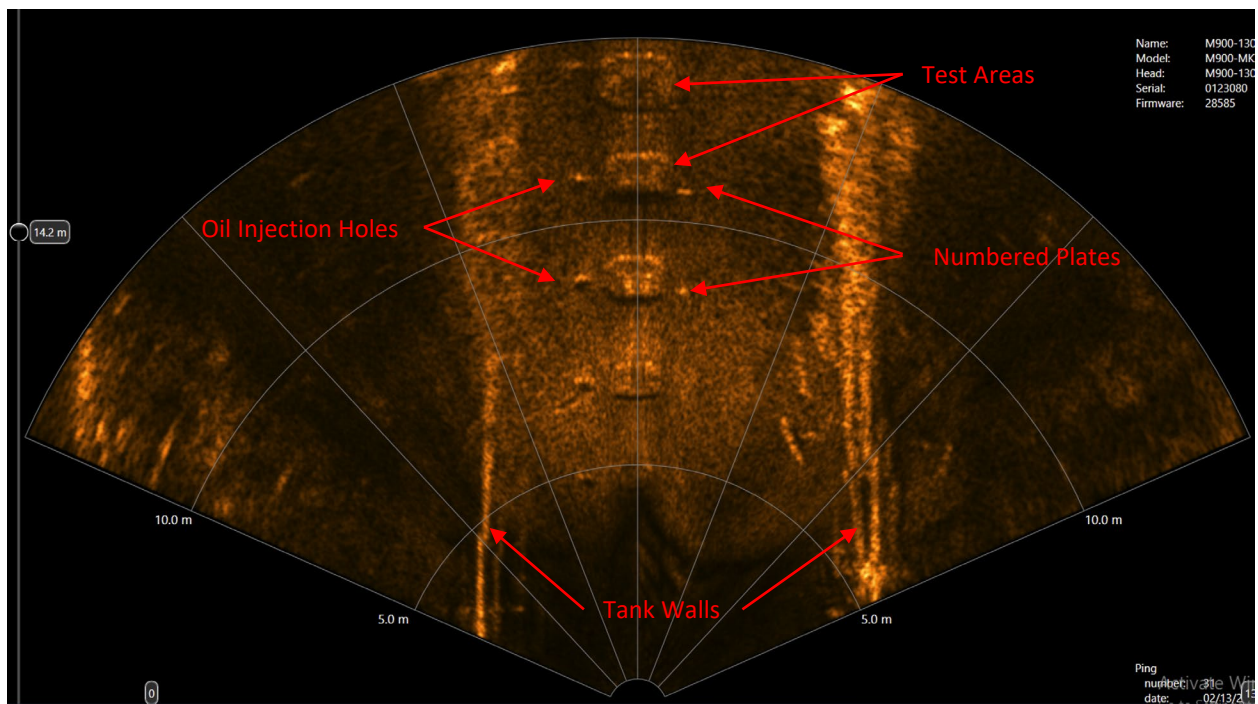


Figure 11: Identifiable features below ice sheet from imaging sonar

Due to these effects described above (and perhaps counterintuitively), static images from the BlueView imaging sonar were not as useful for detecting oil as moving images. Initial viewing of the images did not show obvious variations in acoustic backscatter intensity that could be attributed to the oil layers in Test Areas 2 through 6; however, subsequent processing of the images especially in a moving reference frame by reviewing them in sequence as the sled moved down the tank revealed i) areas of significantly lower acoustic backscatter in the middle of Test Areas 4 through 6 (the most visible to the sled) and ii) a line of high acoustic backscatter along the track of the sled that was likely due to bubbles introduced under the water by the towing lines, which entered and exited the water repeatedly. These processing and visualization techniques developed and tested for this study were exploratory and seem to offer promise for improved oil detection when refined and implemented on field data especially when used in the future with variable depth from the ice and different (or perhaps optimized) look angles.

Completion of the test-matrix interference assessments (aka cross-talk) revealed signal contamination between the BlueView imaging sonar and the echosounder (Nortek Signature 1000 ADCP). Interference could be avoided by using trigger signals that enforce interleaved sampling between the two sensors so only one sensor at a time puts sound into the water. These triggers were not implemented in the CRREL payload but were added for Ohmsett testing (see Section 4); at CRREL, interference was prevented by only running one acoustic sensor at a time. The cross-contamination is likely more pronounced at CRREL, with a small tank and hard walls, than it would be in a field situation with a much larger body of water and relatively softer and irregular bottom.

At minimum, the imaging sonar should provide valuable context on ice roughness and discontinuities in the field, based on the test area perimeters being obvious in the tank sonar images. The imaging sonar may provide information on the spatial extent of oil patches out to the maximum range (approximately 100 m) in the field if the oil sufficiently alters the under-ice roughness and acoustic reflectivity (which may be amplified at the shallow grazing angle of an AUV flying close to the ice), or if the oil collects in natural depressions demarked by altered acoustic reflectivity. Further testing in the field, with longer ranges and larger pools of oil is needed to verify this.

In retrospect, it would have been beneficial to reverse the cart direction for some of the runs, to provide views under the ice from different angles; however, this may have exceeded the length of the tether.

3.4.2 Echosounder

The central beam of the Nortek Signature 1000 ADCP was directed upward at the ice surface and measured acoustic backscatter (ABS) in decibels (dB) with distance from the sensor. ABS plotted over time is typically referred to as an echogram. Figure 12 shows the echogram from the stationary sensor below Test Area 6 as it was filled with oil.

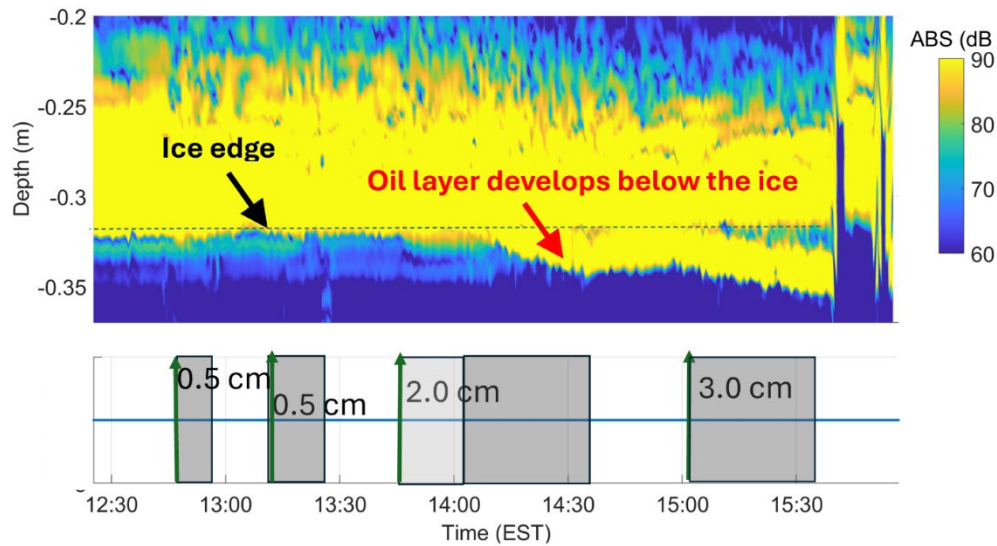


Figure 12: Echogram as Test Area 6 was filled with oil

Timing and amount (as measured by thickness) of oil added to Test Area indicated below

A discernible oil layer developed in the echogram as the third portion of oil was added, after the oil layer was thicker than approximately 1 cm. This observation provides an important measure of this sensor's limit-of-detection (LOD), a key factor that needs to be determined experimentally for any sensing system. As oil continued to be dispensed, a layered feature became apparent in the echogram and continued to separate, eventually becoming fully distinct from the water-ice interface when the oil layer was thicker than approximately 2 cm. This distinctive layering pattern in the echogram is a unique signature of the interfaces between the water, oil, and ice phases, and provides a strong indicator for use in detecting oil under ice and quantifying the oil layer thickness.

Data was collected with the cart stationary below Test Area 4 in the same manner, as shown in Figure 13. The echosounder results at Test Areas 4 and 6 are consistent with previous acoustic-only based oil-detection studies (e.g., Bassett et al., 2014 and 2016) and confirm the sensitivity and broad usefulness of the Nortek Signature 1000 ADCP for this application.

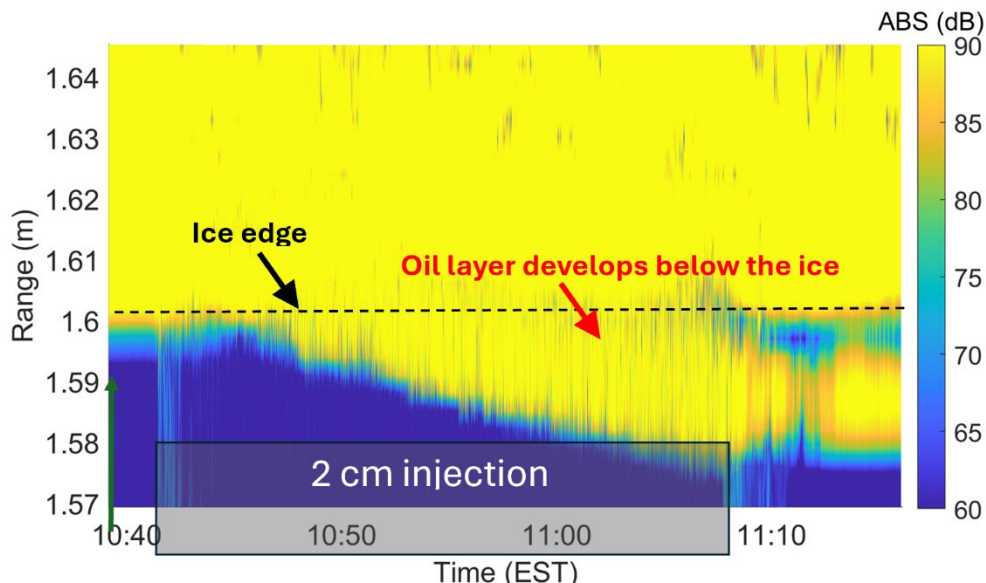


Figure 13: Echogram as Test Area 4 was filled with oil

The next series of tests investigated how well the echosounder could detect oil layers under the ice while moving. Figure 14 shows an echogram while the cart was moved under all six Test Areas, simulating the use of the echosounder on a moving AUV. The echogram shows two prominent features:

1. A convex shaped ‘hump’ which reflects the combination of bathymetry (or the shape of the tank floor which is slightly deeper in the middle of the tank), and the ice being about 10 cm thicker in the middle of the tank than at the ends
2. Increased separation of the layers toward Test Area 6 which reflects the fact that the oil layers were thicker at Test Area 6 and thinnest at Test Area 2 (with Test Area 1 as the control)

The data from the echosounder could be corrected for the change in depth using the on-board pressure sensor. For example, Figure 15 shows the echogram as the cart was moved across the tank, pausing beneath each test area for one minute.

Note that although all echograms reported here show depth on the y-axis, this distance estimate is derived using a constant sound speed and hence is linearly proportional to the measured time delay by the sound pulses from the ADCP. The distance estimates are not corrected for variations in the sound speed in the three different mediums involved (i.e., water, oil, and ice) and therefore are only approximate.

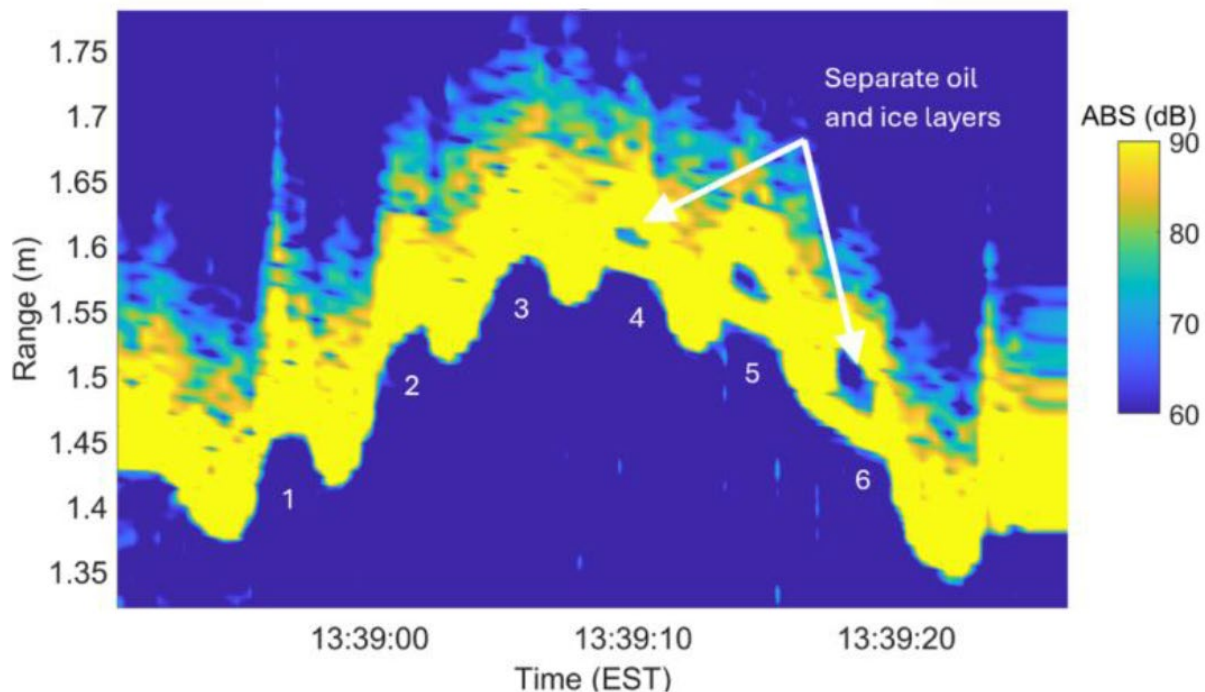


Figure 14: Echogram collected as the sensors moved across the tank
Test Area numbers noted

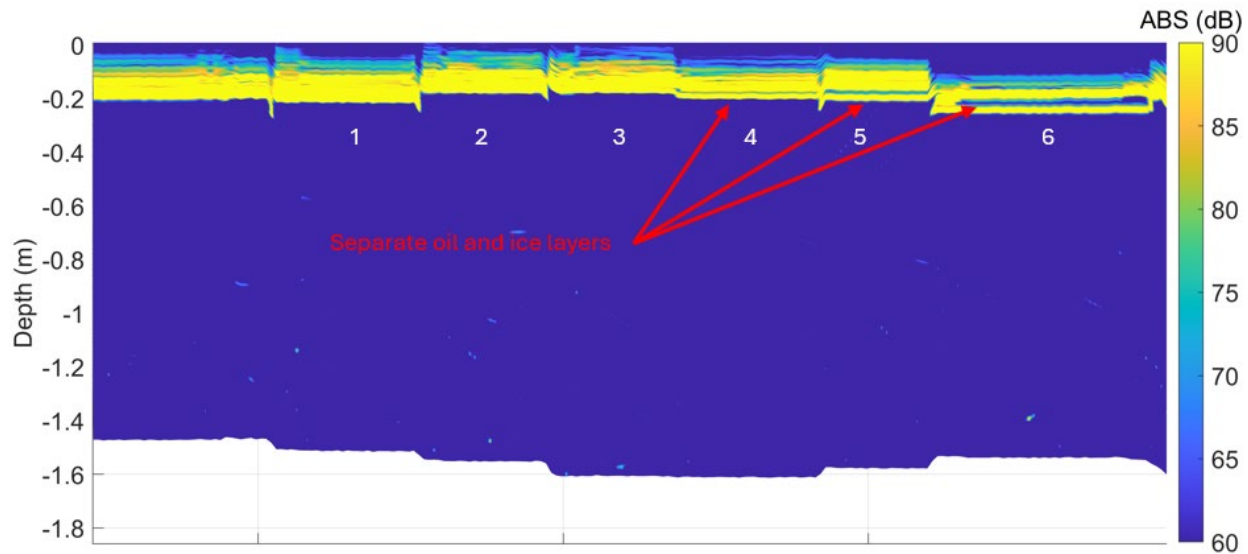


Figure 15: Echogram corrected for depth using pressure sensor data
Test Area numbers noted

The results validate the intended use of the Nortek Signature 1000 ADCP as an echosounder on a moving AUV to detect the presence of oil under sea ice. In summary, the echosounder was able to distinguish between the control Test Area and the test areas with thicker oil layers, returning two distinct reflected signals from the oil/water and oil/ice interfaces. The separation between return signals increased with oil thickness. The sensor performed well stationary, as expected based on prior work, but also while moving, a significant finding of this work.

3.4.3 Camera

The upward looking camera system (PHX122S-MC-IC monochrome camera and TRIO54S-CC color camera) was in operation in most test runs except when powered off to evaluate electrical interference with other sensors. Early testing with the SeaLite LED floodlights showed increased electrical noise on other sensors (particularly the echosounder), and that the supplemental lighting did not materially improve the image quality during daytime testing. As such, they were not used outside of the night testing on February 14th, 2024.

During preliminary testing of the sensor package, both the high-dynamic-range color and monochrome cameras were used. The black and white camera provided sharper, higher resolution images of the underside of the ice and test areas (see Figure 16) while also offering faster shutter speeds, which reduced blurring while the cart was moving, and adequate dynamic range even when strongly backlit. Based on these observations, the monochrome camera was used for most of the remaining tests at CRREL.

During nighttime testing on February 14, 2024, the floodlights were used to illuminate the test patches from below (see Figure 17). As noted above, electrical noise from the lights interfered with the acoustic instruments, however, there was only a marginal gain from testing the acoustic instruments at night. The onboard lights provided excellent illumination of the under-ice surface when needed. The test range was limited to the depth of the tank and the effectiveness in the field will be limited by depth and water clarity. The use of lights under the ice at night may be a

useful technique to identify oil deposits from above (see Figure 18). This technique was also applied successfully with a diver holding lights under the ice during a Canadian experimental oil spill under sea ice in 1980.

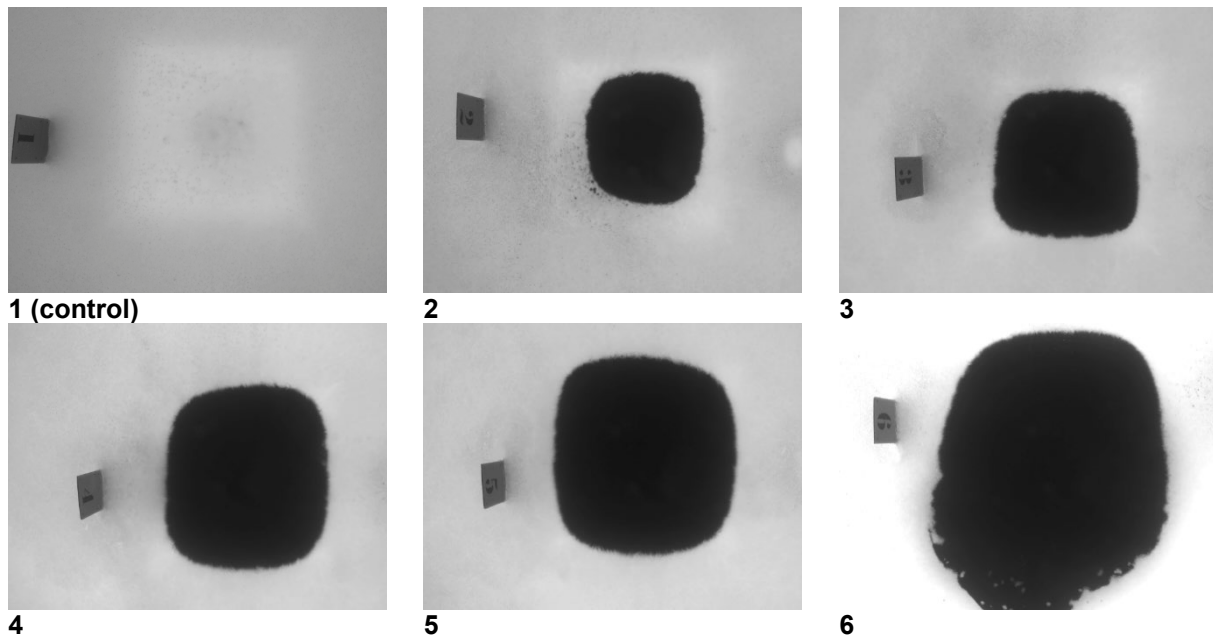


Figure 16: Test areas viewed from below with the monochrome camera

Test area numbers as noted. Images captured during daylight testing, backlit with natural sunlight, on February 13, 2024, six days after injecting oil.

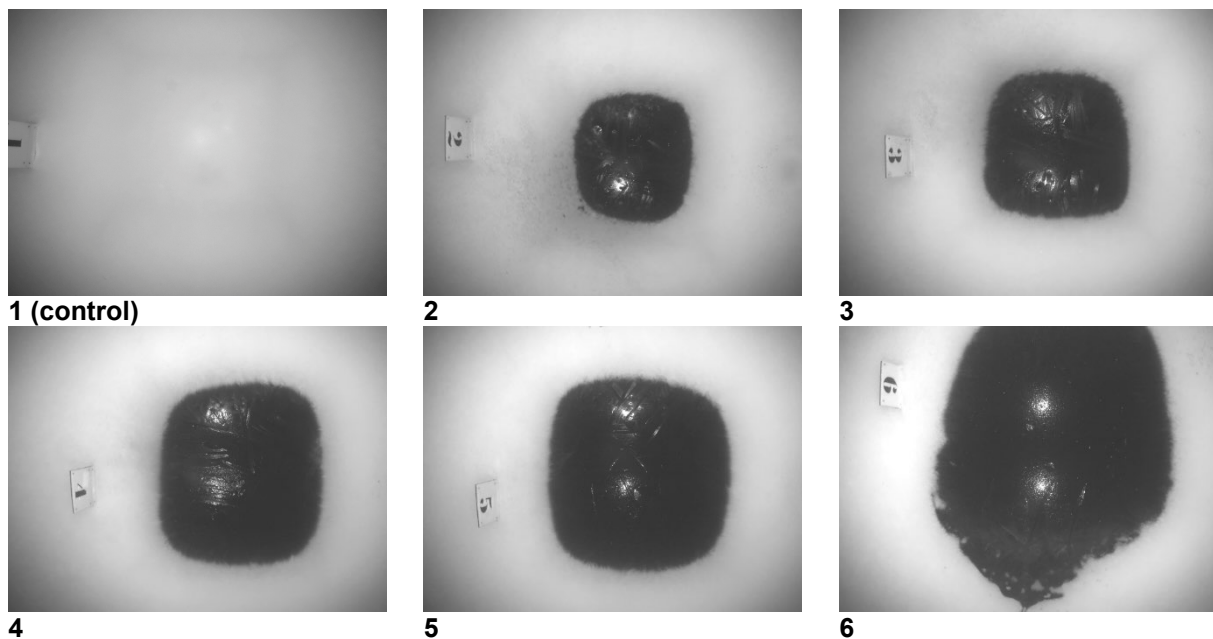


Figure 17: Test areas at night, illuminated by SeaLite LED floodlights

Test area numbers as noted. Specular reflections from floodlights visible on the undersurface of the oil.



Figure 18: Test areas illuminated from beneath the ice with Sealite LED floodlights

3.4.4 PAR

The photosynthetically active radiation sensor (Biospherical MPS-PAR) was extremely sensitive to variations in light level; clouds passing overhead and shadows from people walking past the Test Areas were easily discernible. Figure 19 shows the scale of light intensity that was measured by the PAR between nighttime and daylight conditions. The PAR also worked well in low light conditions on the evening of February 14, 2024; ambient light from nearby streetlights and the moon were sufficient to discriminate from measurements when the sensor was below an oil pool and when it was between test areas.

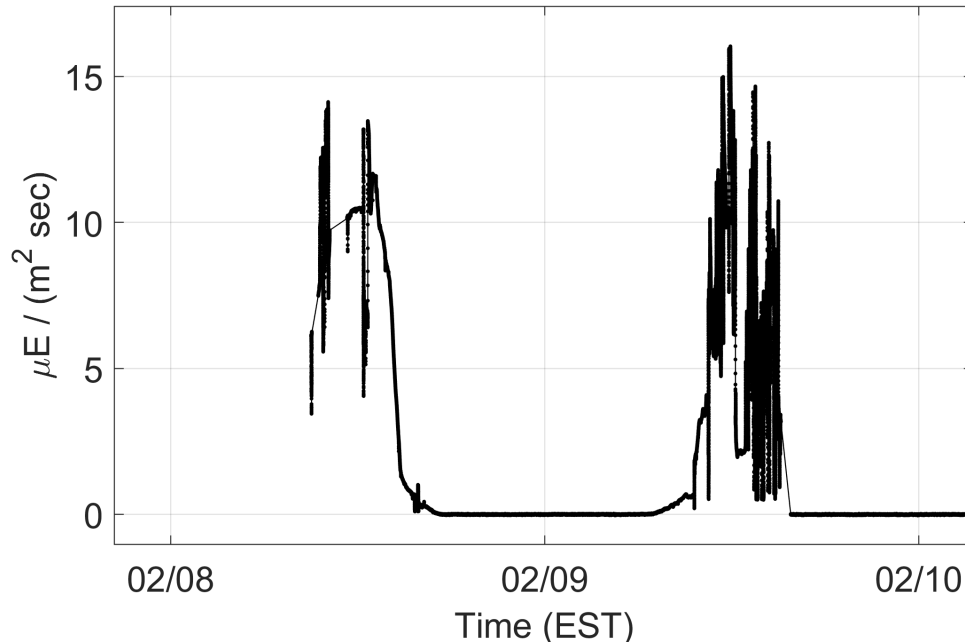


Figure 19: PAR measurements from beneath ice over 48 hours

Figure 20 shows the PAR signal as the cart was moved across the tank. The reduction in light intensity from the oil in the test areas is evident and significantly greater than the natural variation in light attenuation from the ice. An example of a simple method to analyze the signal from the MPS-PAR that could be applied is to subtract the background or ambient light level at a given depth and then rescale the measurements using the maximum measured radiation level (see Figure 21). The data shows the test areas with oil have a significantly stronger signal than the control test area.

Optical detection with the PAR was more sensitive and capable of detecting thinner (< 1 cm) oil layers than the acoustic methods that were used and should be very useful to detect the edges of oil pools in the field. No snow or other precipitation fell on the ice during the two weeks of testing, so the conditions of the ice sheet were very consistent across the tank. Further testing in the field with natural ice and snow would provide useful information on expected natural variation in light transmission to compare with these results.

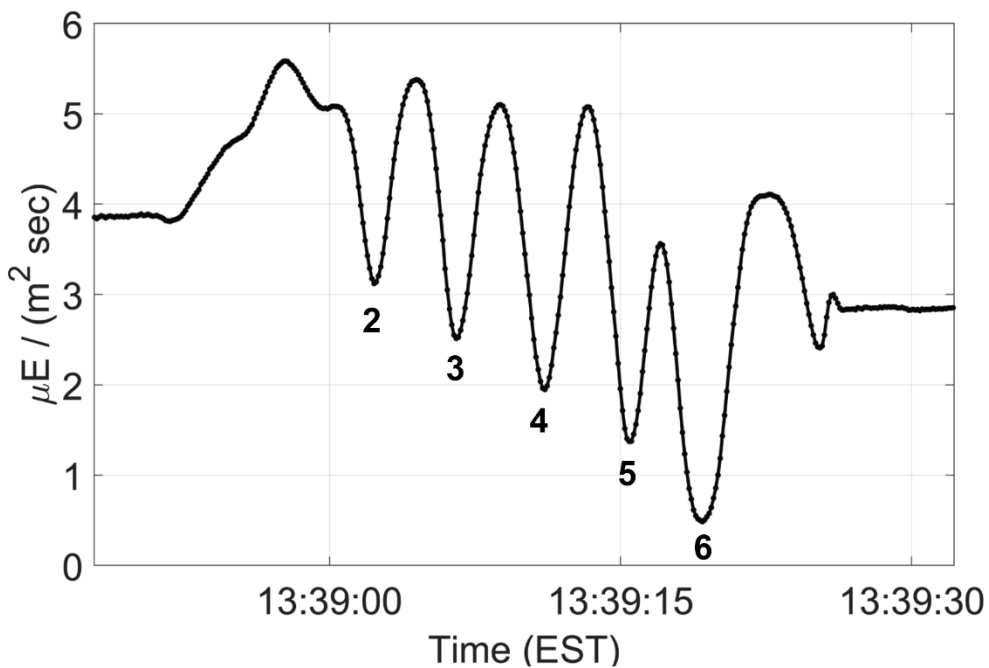


Figure 20: PAR measurements as sensor moved across tank

Test area numbers as noted. Maximum radiation corresponds to Test Area 1 (control) and regions between oil pools, while minimums are measured beneath oil pools.

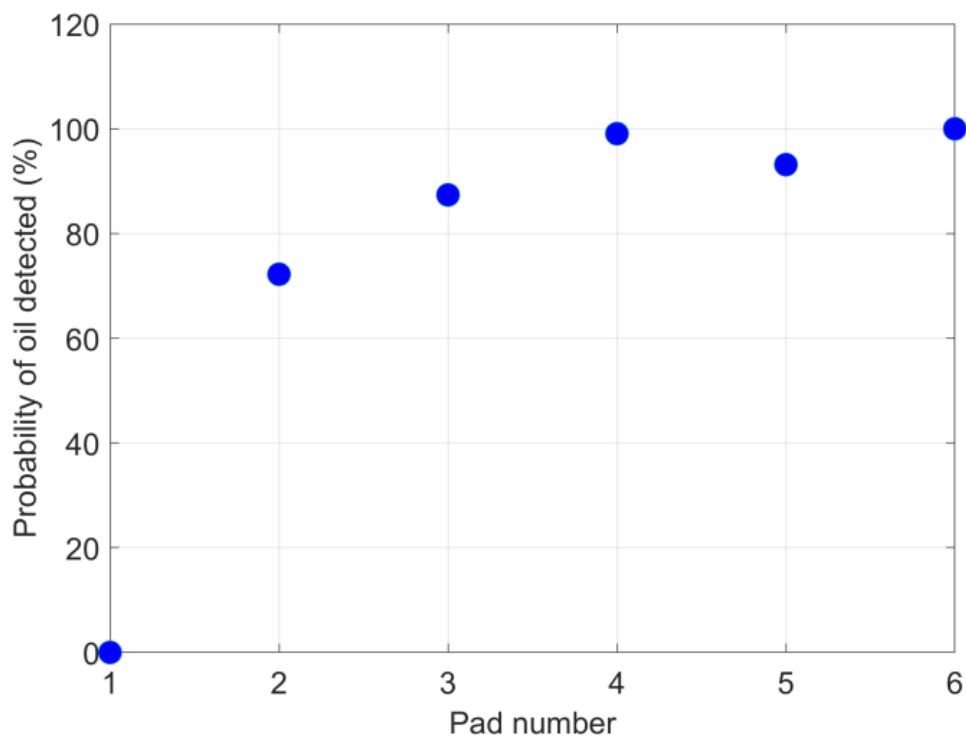


Figure 21: PAR data analyzed to identify minimum values corresponding to oil pools

Oil index scaled based on average maximum (background) and minimum PAR measurements

3.4.5 UV Fluorometer

The ability to test the Chelsea Technologies UviLux fluorescence sensor was limited due to the CRREL GRF tank being a closed system. Measured concentrations of PAHs were noisy with a relatively high background concentration, presumably due to previous tests with crude oil in the tank. An approximately 10% increase in concentration ($\sim 0.5 \mu\text{g/L}$) above the initial measurements was noted after adding oil to the Test Areas on February 9, 2024 (see Figure 22).

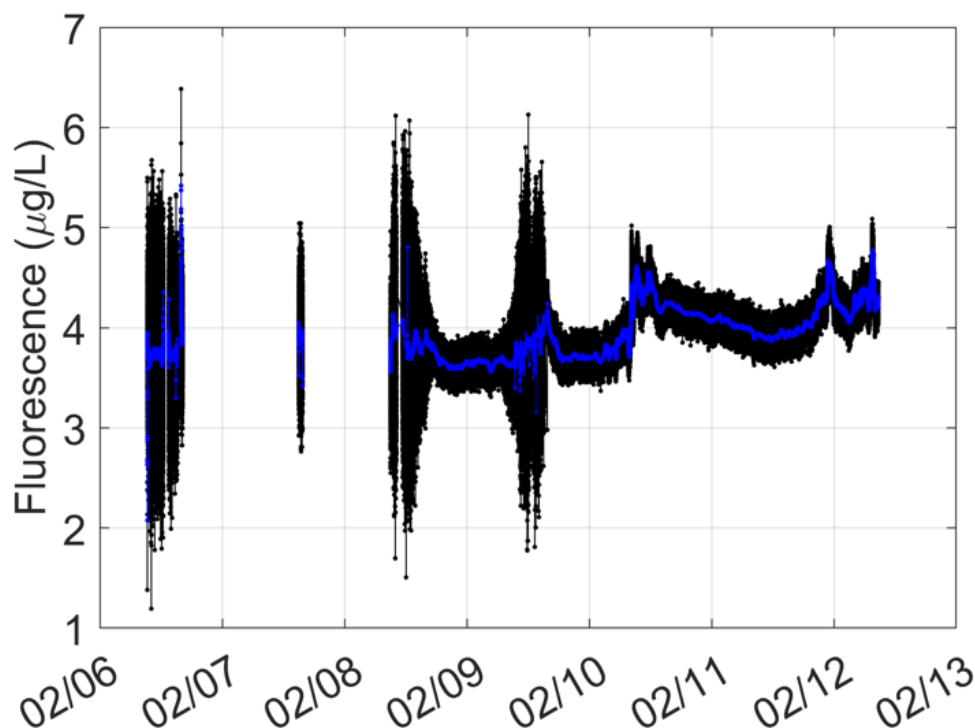


Figure 22: UV Fluorometer measurements before and after oil was distributed

Raw measurements shown in black, moving average in blue

Adding a second UV fluorometer calibrated to detect BTEX compounds may help to detect lighter oils, which typically have higher concentrations of light aromatics. Further testing in the field with expected lower background concentrations would be useful.

4 Submerged Oil Tests

The sensor package was tested at the BSEE Ohmsett facility with submerged oil targets. The objective of the experiments was to evaluate the ability of the combined sensor package to identify and characterize oil targets that were submerged at the bottom of the tank on a sandy substrate. The experimental methodology was follows:

- Deploy several types of heavy oil targets with varying presentations at the bottom of a test basin
- Mount the sensor package on a ROV and AUV and maneuver the vehicles around the tank under their own power
- Operate the sensors through the vehicle interfaces and gather data on the submerged oil targets
- Assess the ability of the sensors individually and collectively to identify submerged oil

The submerged oil tests were carried out between June 3 and 7, 2024.

4.1 Facility and Equipment

The submerged oil tests were completed at Ohmsett, the National Oil Spill Response Research and Renewable Energy Test Facility, which is located on the grounds of Naval Weapons Station Earle in Leonardo, New Jersey. The tank measures 200 m long, 20 m wide and 2.5 m deep, and was filled with salt water (salinity 28‰).

4.1.1 Test Oils

Three different heavy oils were used during the tests, as summarized in Table 10. Barite or barium sulfate (Haliburton Baroid 41 drilling mud) is a naturally occurring mineral with a density of 4.5 g/cm³. Small amounts were added to some of the test oils, as described below, to increase the density and ensure they remained submerged. The presence of barite in the oil samples would not affect the response from the sensors.

4.1.2 Submerged Oil Targets

Twelve submerged targets were prepared using fiberglass pans (McMaster Carr 41025T26) that measured 120 cm long, 61 cm wide and 6 cm deep (47 1/2 in. by 24 in. by 2 1/4 in.). Fiberglass has significantly lower acoustic reflectivity than metal to avoid contamination of the acoustic sensors but sufficient structural strength to allow the samples to be raised and lowered into the tank.

Two of the pans were left empty and used for acoustic referencing and interference purposes, while the remainder were each filled with approximately 55 kg of washed and screened playground sand (Sakrete Play Sand, D50 = 0.45 mm) mixed with 0.9 kg of Portland cement (Sakrete Portland Cement Type I-II) to provide structure and prevent sand from being washed out of the pans during placement or by the ROV propellers. The pans were filled to an average depth of 5 cm (2 in.), with a circular depression in the center measuring (15 in.) in diameter and 2.5 cm (1 in.) deep (see Figure 23). The contents of each test pan is described in Table 11.

Table 10: Oils used in submerged oil tests

Test Oil	Description and Properties
Tesoro Decant Oil	Also called Cat Cracked Slurry Oil, this is a residue product from the catalytic cracking process at refineries. Several spills of oil that sank involved this type of oil (API 2016). The oil was liquid at room temperature and denser than the Ohmsett tank water. The oil has an unusually low viscosity for a heavy oil and the project team was concerned that it might wash out of the tray when it was lowered into the tank. To prevent this from happening, the team added 0.5 kg barite to the oil to increase its viscosity prior to applying it to test pans 9, 10, and 11.
Roofing Cement	Roofing cement was chosen as an analog for a heavy fuel oil, such as Bunker C or Number 6 Fuel Oil. The product used is an emulsion of asphaltenes (40 to 50%), mineral spirits (8 to 20%), cellulose (2 to 6%), and bentonite (10 to 25%). These constituents would be similar to a tar ball with inclusions of natural mineral and organic matter. The product was semi-solid at room temperature and was slightly buoyant in Ohmsett tank water. The project team added 1.2 kg barite to 16.6 kg of heated roofing tar to increase its bulk density prior to applying it to the test pans.
Hibernia Crude Oil Burn Residue	Burn residue from laboratory burn tests with Hibernia Crude Oil was prepared by SL Ross Environmental Research. The residue was semi-solid at room temperature and sank in Ohmsett tank water. The burn residue was heated to 60°C in a water bath to improve workability before applying it to test pan.



Figure 23: Pans filled with sand and cement mixture

Ten of the twelve test pans had eight visual fiducial markers attached to the outer rim, laying flat on the tank floor to minimize acoustic interference. The tags are made from a composite layer of plastic sheet and thin aluminum foil (Dibond) each printed with a unique fiducial pattern using the Apriltag system, mounted to an acrylic backer. The codes on the tags can be detected during post processing of the onboard camera images and allow automated identification of the sample trays and accurate determination of the position of the underwater vehicle and look angle of the

sensors relative to the submerged oil targets. Some pans were deployed without tags for data quality control purposes. Several pans are shown prior to deployment in Figure 24.

Table 11: Test pan contents and appearance

Pan #	Substrate	Fiducial Markers	Oil	Description
1	Empty	No	No	Control test pan, baseline
2	Empty	Yes	No	Control test pan, to assess potential of acoustic interference from the tags
3	Sand	Yes	No	Control test pan, to assess acoustic signature of the substrate without oil
4	Sand	Yes	2.5 kg Tesoro Decant Oil	Oil was observed to infiltrate into sand below and around depression. Only small amount of liquid oil remained above sand.
5	Sand	No	No	Control test pan
6	Sand	Yes	4.9 kg Roofing Tar	Roofing tar was smoothed out to the edges of the depression.
7	Sand	Yes	7.3 kg Roofing Tar	Roofing tar was smoothed out to the edges of the depression. Presentation was dome-shaped.
8	Sand	Yes	4.4 kg Roofing Tar	Roofing tar was smoothed out to the edges of the depression. Spread approximately 1.5 kg of sand across top of tar.
9	Sand	Yes	3.1 kg Tesoro Decant Oil mixed with 0.5 kg Barite	Wet sand in tray before applying oil. Oil did seep into sand around depression, but less than with tray 4.
10	Sand	Yes	3.1 kg Tesoro Decant Oil mixed with 0.5 kg Barite	Wet sand in tray before applying oil and built-up sand lip around depression. Oil remained in place better than with trays 4 and 9.
11	Sand	Yes	3.1 kg Tesoro Decant Oil mixed with 0.5 kg Barite	Wet sand in tray before applying oil. Spread approximately 1.5 kg of sand over oil, which mixed into the oil layer.
12	Sand	Yes	1.5 kg Burn Residue	Burn residue covered ~90% of the bottom of the depression.

The pans were carefully lowered into the tank using the crane on the Main Bridge. The targets were placed close to the center line of the tank, extending over about the middle half of the tank length (see Figure 25). The underwater robotic vehicles were driven up and down the tank, over the targets, to gather data with the sensor payload.



Figure 24: Pans with visual markers and test oils

Upper Left: Pans 9, 10 and 11 before oil was added. Middle: Pan 12. Right: Pans 6, 7 and 8.

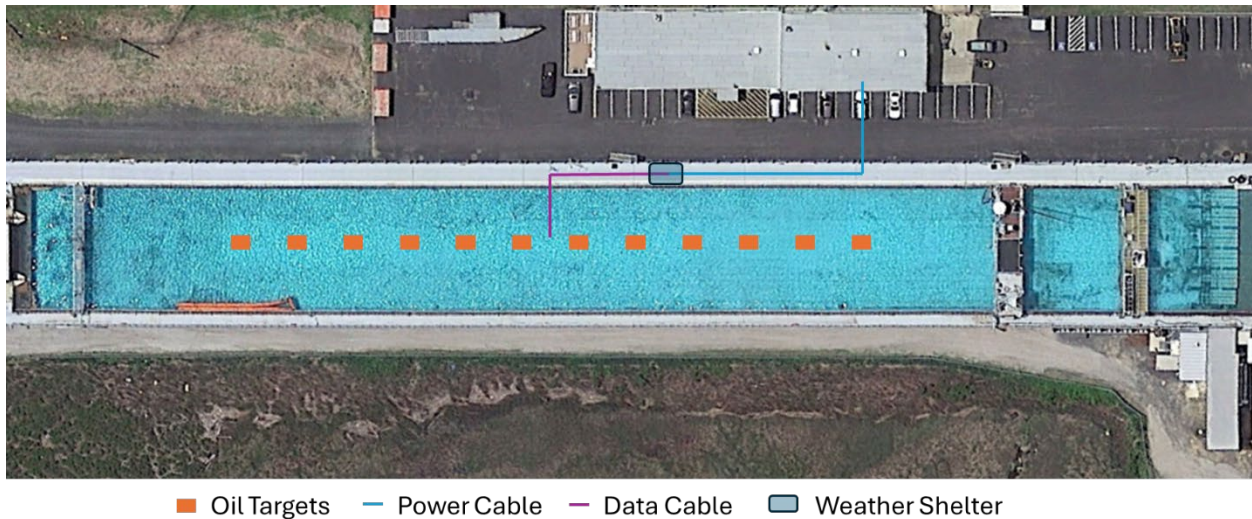


Figure 25: Submerged oil pan layout at Ohmsett

4.1.3 Underwater Platforms

The sensor package was mounted on two underwater platforms during the tests (see Figure 26):

1. a UW/APL Raven ROV
2. a Hydroid Inc. Remus 100 AUV

The Raven ROV was designed and built at UW/APL for the testing of novel perception sensors and autonomy algorithms. At approx. 175 kg in-air weight, it can be deployed from vessels of opportunity with a suitable crane or davit, power, and space for piloting equipment. A key feature of the Raven ROV is its hybrid copper/fiber optic tether which provides 2400 W of power for propulsion and sensors as well as 10 Gbit ethernet connectivity, allowing uplink of

high-bandwidth, uncompressed sensor streams to shoreside operators. The native control software has been further extended by UW/APL-developed software written in the Robot Operating System (ROS) and allows straightforward addition of novel sensors and testing of autonomy algorithms running either onboard the vehicle or on support computers on the surface. The Raven is designed for shallow-water operation, with a maximum depth rating of 100 m. In its standard configuration the vehicle has approximately 13 kg of spare buoyancy capacity and 400 W of payload electrical power.

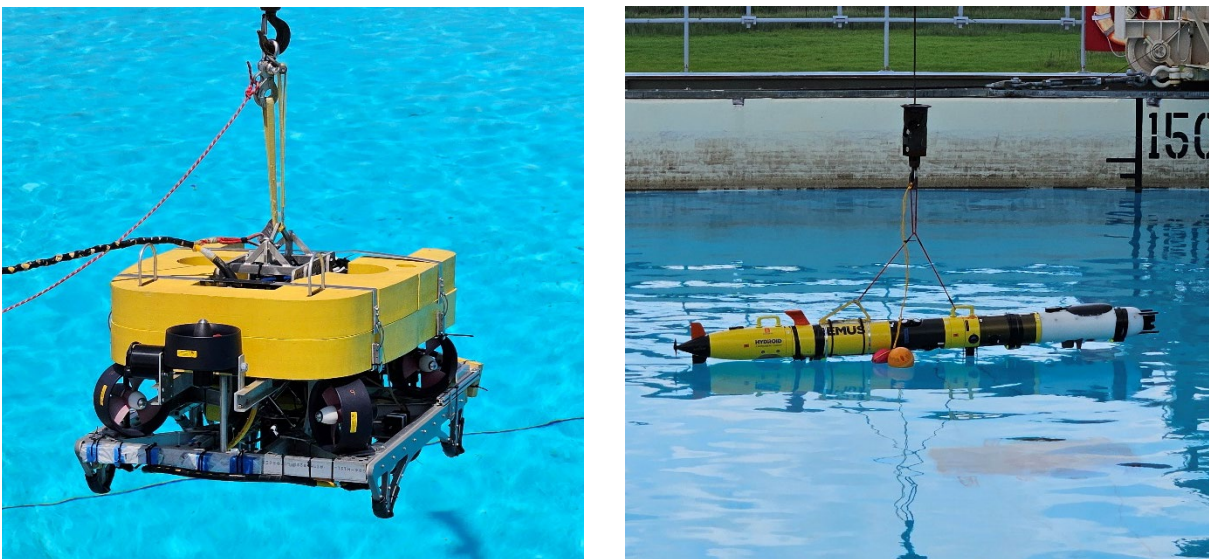


Figure 26: Underwater platforms used at Ohmsett
Left: UW/APL Raven ROV. Right: Hydroid Inc. Remus 100 AUV

The Remus 100 AUV is built by Hydroid Inc. (currently owned by Huntington Ingalls Industries). The vehicle measures 2 m in length with a 20 cm outer diameter (OD) and can be deployed by a two-person team. The Remus 100 AUV has a top speed of 1.8 m/s (3.5 knots) and a working depth of 100 m. The onboard batteries give it a mission duration of approximately 12 hours, based on previous experience by UW/APL. The sensor payload module was installed on the front of the Remus 100 AUV and interfaced with vehicle power and data. Sensor data was stored onboard and downloaded after missions.

The Remus 100 AUV has several other sensors that were operated in addition to the oil detection payload of sensors. These included two independent conductivity, temperature, and depth (CTD), marine optical sensors for phytoplankton pigments and colored dissolved organic matter (CDOM), and dissolved oxygen (DO).

4.2 Test Parameters

As with the Task 5 tests at CRREL, a test matrix was developed for OHMSETT to ensure a high-quality data set that would allow the project team to: i) assess interferences between the sensors, ii) evaluate environmental noise in the test tank, and iii) quantify the effect of the apparatus (i.e., trays, sand and cement substrate, fiducial markers) used to contain the oil samples on the sensor measurements. A summary of all missions is shown in Appendix D, including reporting time of

data collection and data type for each payload section and a brief description of each test along with a reference to the identification number for the sensor configuration contained in the text matrix.

For these purposes the control test pans were closely studied after the vehicles were operational. Particular attention was given to potential acoustic interference with the fiducial markers since these were not used at CRREL. The first (and sometimes second) deployment of each vehicle was used to optimize sensor performance based on real time and post analysis of the data. Some examples of optimizations performed on site included:

- adjustment of the lookout angle of the BlueView imaging sonar on the Raven ROV
- cleaning of the camera windows
- changing camera exposure settings to reduce overexposure
- reducing the power of the central beam on the Signature 1000 ADCP and piloting the Raven ROV near the surface of the tank to avoid echosounder saturation at the sample interface

These adjustments were important to the effective operation of the sensors, and similar tuning may be required during field operations. Other observational parameters were altered throughout data collection including vehicle depth, view angle, and distance between the target and the sensor. Intensive sampling was performed at the most important test pans by actively moving the Raven ROV upwards, downwards, and around the test pan to capture data for use in rendering a full 3D view of the tray and the oil samples within them during post-processing.

4.3 Observations

Observations made during the tests at Ohmsett are presented below.

4.3.1 Weather Conditions

Weather conditions were generally favorable during the week of testing at Ohmsett, as summarized in Table 12.

Table 12: Weather conditions during testing at Ohmsett

	Mon	Tues	Wed	Thurs	Fri
	Sunny	Sunny	P. Cloudy	P. Cloudy	Sunny
Low (°C)	23	20	19	21	20
High (°C)	31	27	27	30	31

4.3.2 Remus 100 AUV Operation

The project team experienced issues with the onboard navigation for the Remus 100 AUV and were unable to have it self-pilot within the tank. It is possible that the structure of the tank, for example the steel in the bridges, rails, and concrete, interfered with the internal compass. Several missions were done while towing the Remus 100 AUV down the tank with an inflatable dinghy, to simulate normal operation.

4.4 Sensor Results

Results from the sensors used at Ohmsett are discussed below.

4.4.1 Imaging Sonar

The BlueView imaging sonar provided broad underwater views of the tank, with clear images out to at least 50 m (see Figure 27). Fine details of the submerged oil targets were visible. For example, the edges of the pan and fiducial markers showed up as bright, indicating high reflectivity, and the heavy oil showed up as dark, indicating low reflectivity. Also visible is an acoustic shadow cast by the further edge of the test pan. The surrounding concrete floor of the tank showed different acoustic reflectivity than the test pans. The long sensing range would be very useful in the field during a spill response.

As an example of using the BlueView imaging sonar for remote oil detection, the acoustic backscatter from each test pan was analyzed when the sensor was 5 to 10 m from the sample pans on the tank floor. As described in Table 11, a test pan may have oil, no oil, or buried oil. A simple statistical detection algorithm was used to assess the difference in acoustic backscatter intensity between the sample patch in the middle of the pan and the sand substrate surrounding the sample patch. This approach is analogous to measuring backscatter intensity in an area where there is no oil (e.g., as the sensor platform is moving from the deployment area to the spill site) and comparing it to measurements from the area where oil may be present. An area with significantly lower backscatter intensity may indicate the presence of oil.

Randomly distributed measurements ($N=10$) of the replayed acoustic backscatter intensity from the acoustic images taken on the Raven ROV within both regions of the pan were taken (by hand using computer mouse). The mean value was used as the ‘signal’ and the standard deviation was used as the ‘noise’. The total error for detectability was taken as the sum of the standard errors for each sample and the signal-to-noise ratio was calculated (by division) for each pan. The method can accommodate variations in range from the sample and viewing angle (within reason) since both the central patch and the surrounding sand region are both subject to the same intensity variations due to those factors.

For the first trial of the algorithm, the threshold for identifying the presence of oil was set to when the signal-to-noise ratio (S/N) was greater than one. The quality-controlled results were plotted in for each test pan in Figure 28. The algorithm correctly identified the presence of oil ($S/N > 1$) in all test pans with oil, except for Test Pan 8, where the oil was buried beneath a thin layer of sand. The algorithm successfully identified the absence of oil ($S/N < 1$) in the control test pans (i.e., Test Pans 1 through 3).

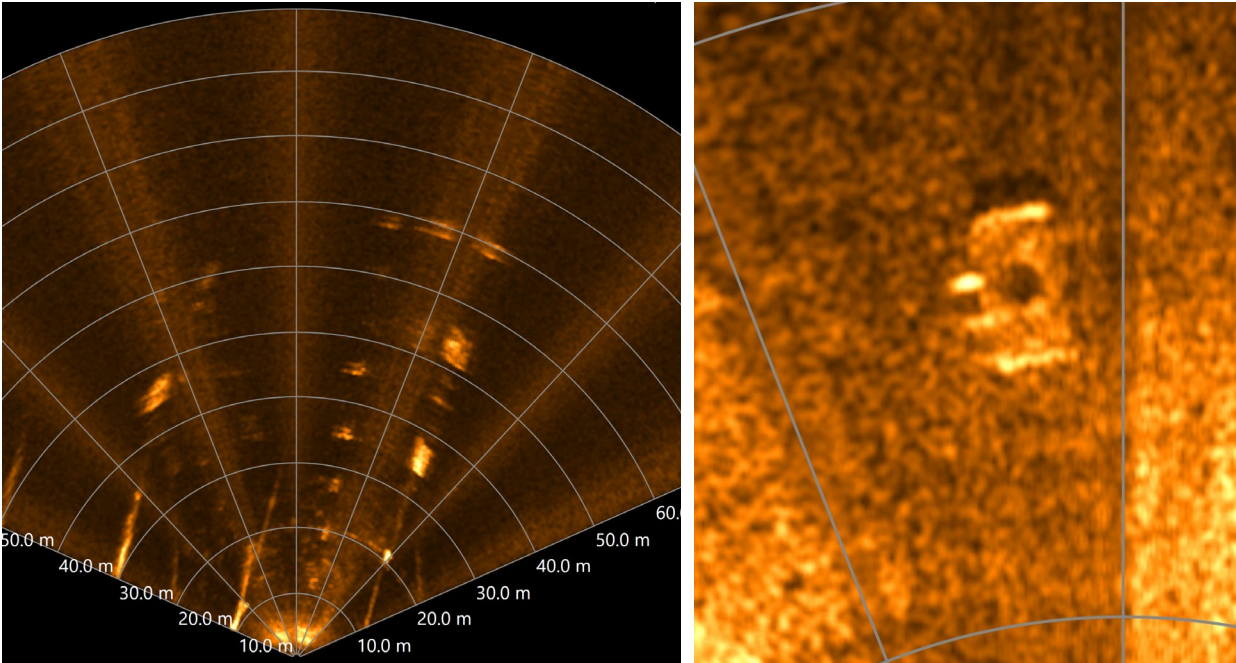


Figure 27: Images from BlueView sonar at Ohmsett

Left: multiple sample trays visible along center line of the tank. Right: zoom showing fine details of sample pans, including reflections from the QR code tags, and lower backscatter intensity of the oil pool in the center.

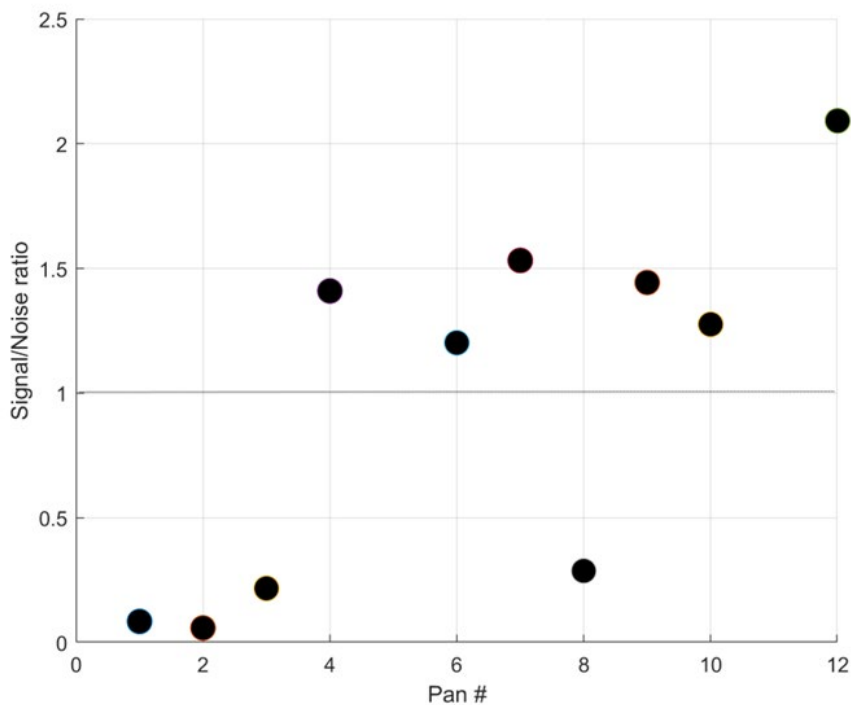


Figure 28: Analysis of BlueView Imaging Sonar results for submerged oil detection

$S/N > 1$ correctly predicts oil was present in test pans 4 through 12, except for test pan 8, which had oil buried under a thin layer of sand.

The threshold for detecting oil can be adjusted by using different values of S/N. Figure 29 illustrates the effect of increasing S/N threshold from 1 to 3 on the identification of the oil. Lower detection thresholds identify the oil but mis-identify areas at the periphery of the field of view and some parts of the substrate in the test pan, while higher S/N thresholds show more detections centered on the oil.

This analysis was based on one frame of the BlueView Imaging Sonar measurements. In a spill response situation, this type of analysis could be run continuously (assuming sufficient available computing power) to identify areas of low backscatter intensity that require further investigation, and even direct navigation of the underwater vehicle. These results strongly support the inclusion of an imaging sonar to provide far-field acoustic imagery for use in real-time oil detection algorithms and eventual mapping of submerged oil on the seafloor in the region of oil spills. Further testing in more natural environments, with more varied and softer interfaces, is needed to improve the accuracy of the oil detection algorithm.

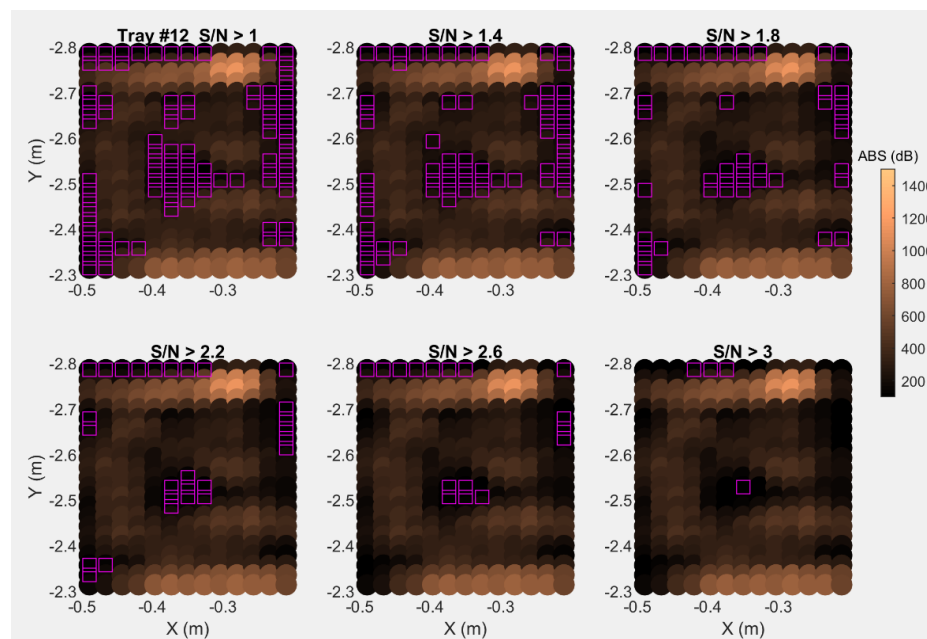


Figure 29: Automatic detection algorithm results for Test Pan 12 varying S/N ratio

Purple square indicates pixel with lower backscatter intensity compared to mean exceeding noted S/N threshold

4.4.2 Echosounder

The upward-looking echosounder (Nortek Signature 1000 ADCP) was able to differentiate oil layers thicker than about 1 cm from the ice sheet at CRREL, returning separate acoustic backscatter signals from the oil/water and oil/ice interfaces. It was not clear whether the same performance would be achieved using the echosounder in a downward-facing orientation with oil on top of a softer substrate.

First, data was collected with the central beam of the echosounder operating in high-resolution mode while the Raven ROV hovered over each sample tray for approximately 1 minute.

Example echograms are shown in Figure 30, Figure 31, and Figure 32. Corresponding monochrome camera images are shown in Section 4.3.3, below.

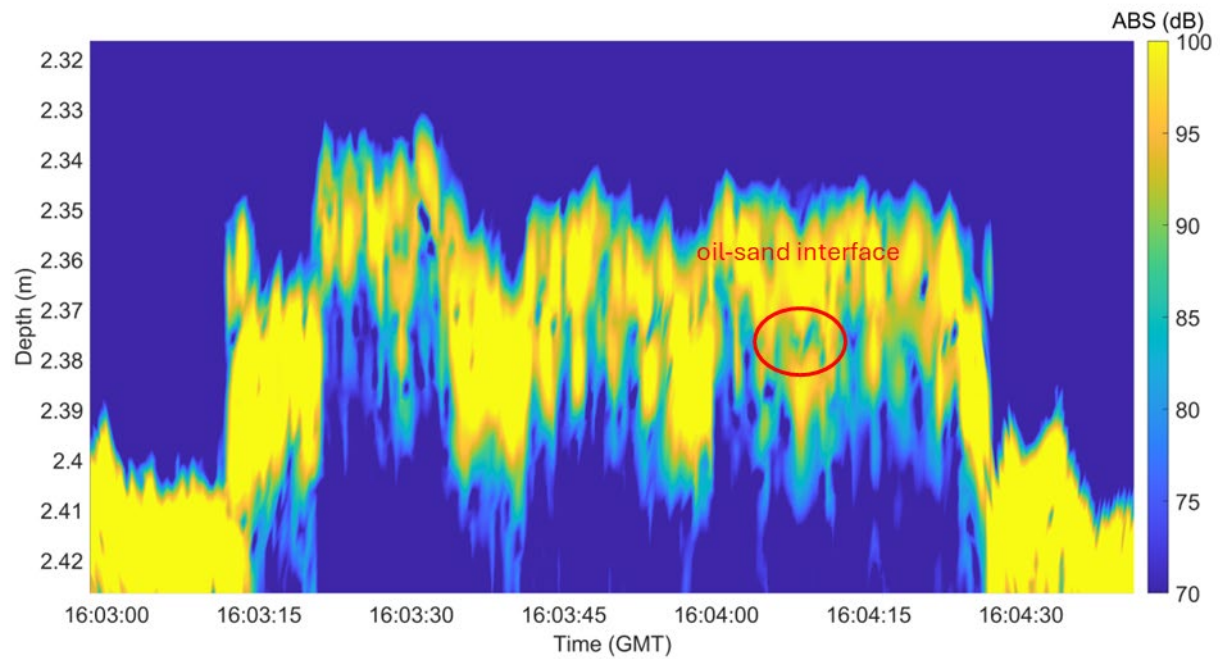


Figure 30: Echogram as Raven ROV hovered over Test Pan 7
Test Pan 7 contained roofing tar. Separate oil/sand interface highlighted.

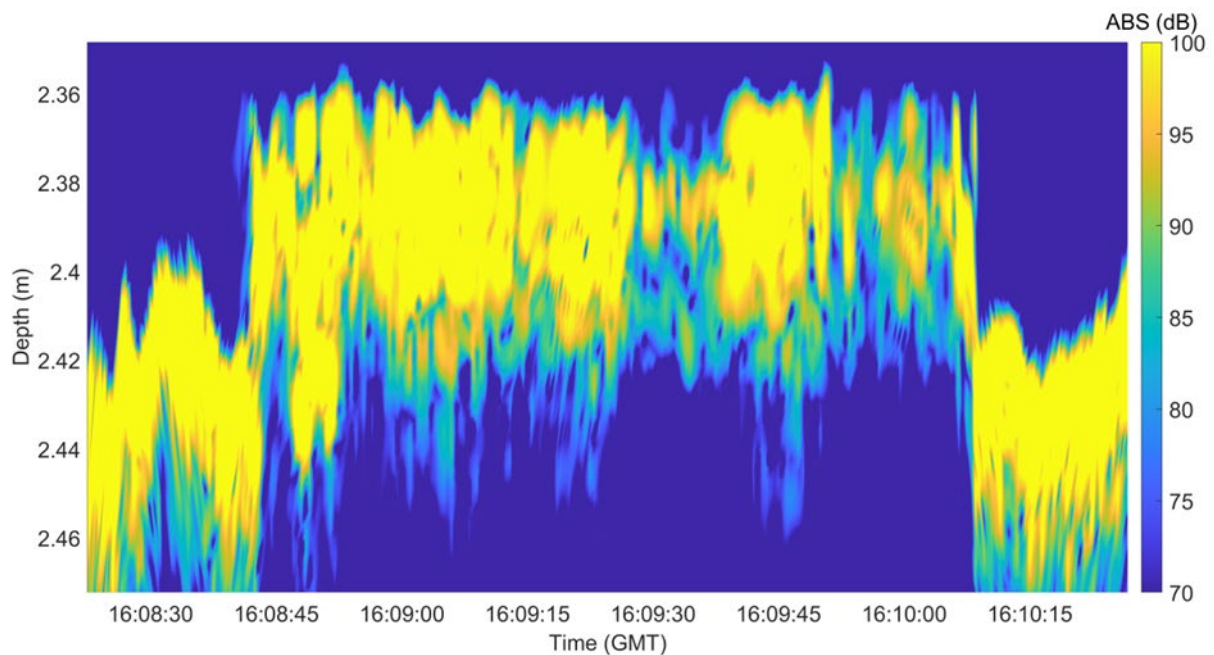


Figure 31: Echogram as Raven ROV hovered over Test Pan 10
Test Pan 10 contained Tesoro decant oil with barite.

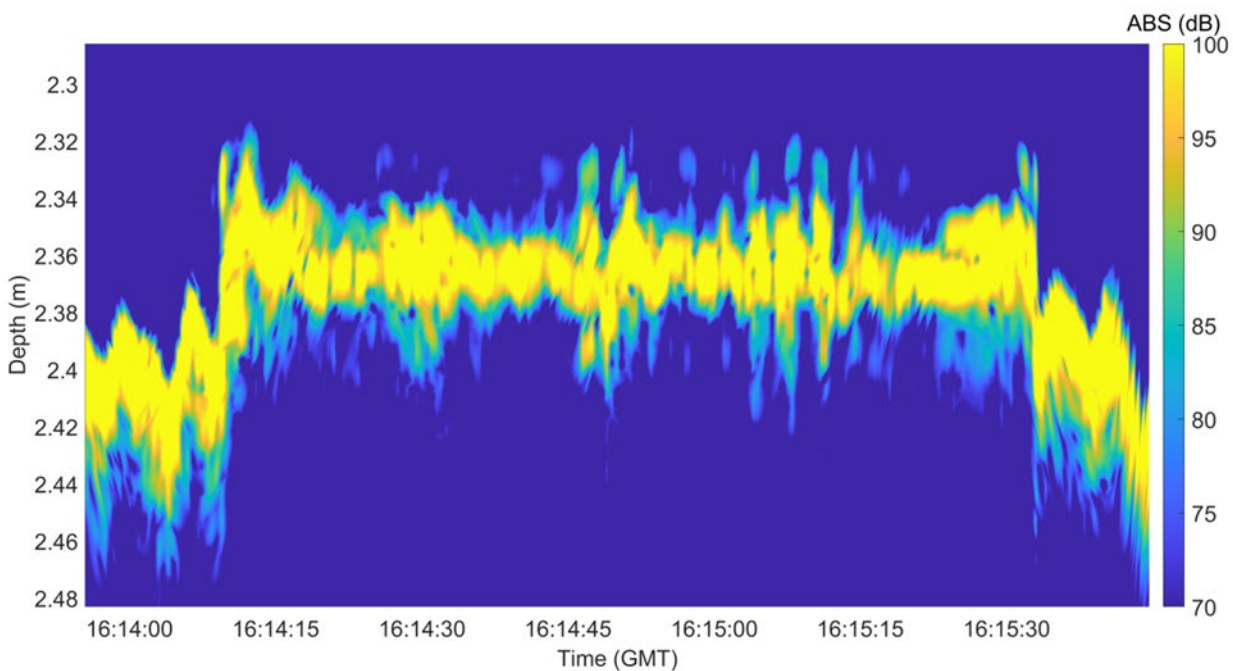


Figure 32: Echogram as Raven ROV hovered over Test Pan 12
Test Pan 12 contained burn residue.

The echogram of Test Pan 7, which contained roofing tar, showed the clearest indication of separation of the oil/water and oil/sand interfaces, as highlighted. The echograms of the Tesoro decant oil (Test Pan 10) and burn residue (Test Pans 12) did not show separate oil/sand interfaces. The oil/ice interfaces observed at CRREL were significantly more pronounced than the oil/sand interfaces observed at Ohmsett using acoustic detection. One reason could be due to differences in density and reflective characteristics between the ice and sand. Another possible explanation could be the slight motion of the hovering Raven ROV relative to the target compared to the cart at CRREL, which was on the bottom of the tank.

The next series of tests were conducted with the Raven ROV making passes down the length of the tank, pausing briefly over each submerged test pan. This simulated using the sensor payload in the field to scan an area for oil deposits. The monochrome camera images collected during the transit were processed to read the fiducial markers on the test pans and determine the position and orientation of the echosounder relative to the test pans. The position-based echograms were assembled in Figure 33, demonstrating how this technology could be used to map an area of interest. Significant layering was noted in some of the test pans with oil (e.g. Test Pans 8, 10, 11 and 12), but was also noted with the empty Test Pan 2. Further investigation of this technique is needed to understand and differentiate between return signals from different interfaces. Tests with more natural bottom substrates are recommended.

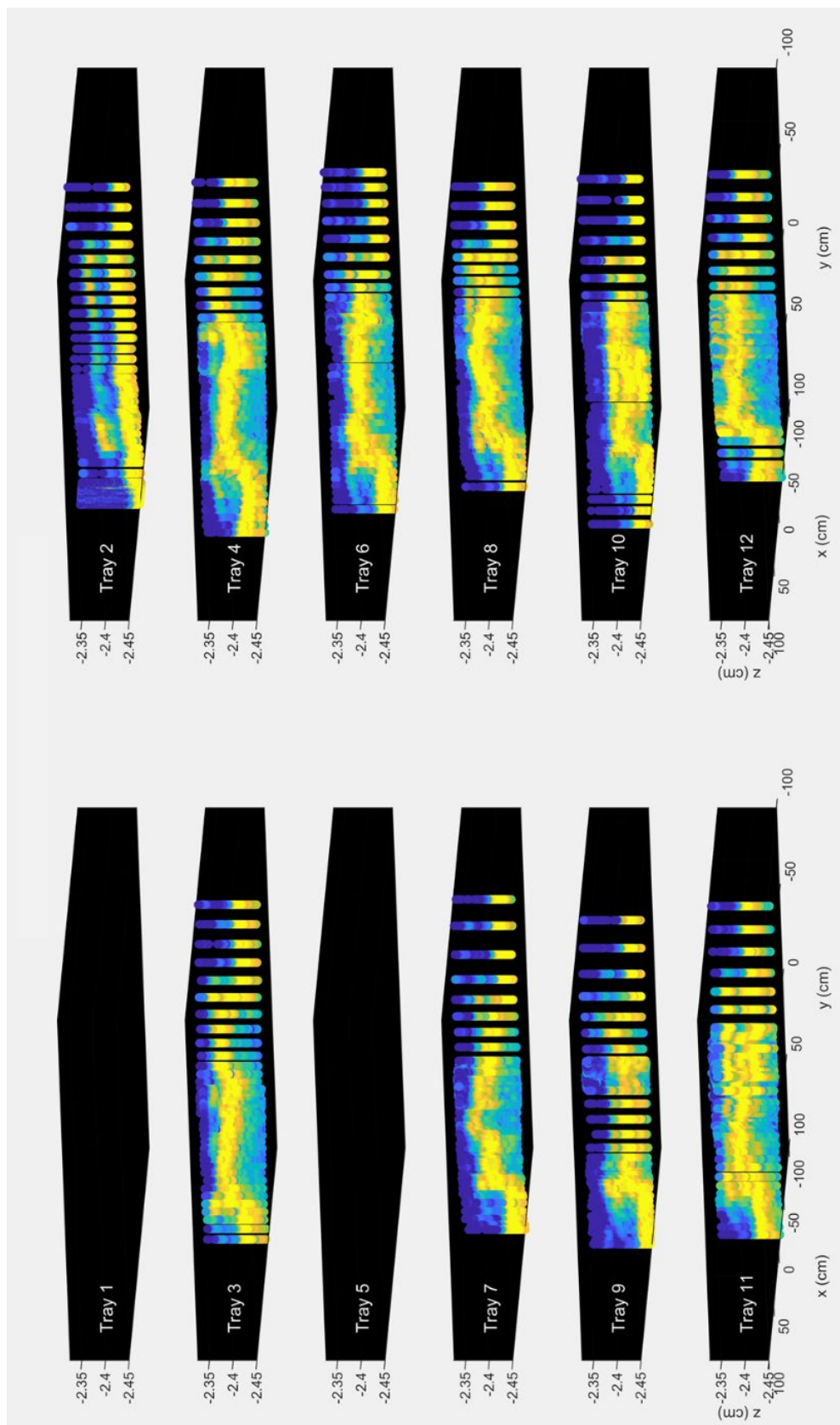


Figure 33: Compiled echograms from Raven ROV transit

Finally, as part of testing the UV Fluorometer, dispersed crude oil was injected into the Ohmsett tank to provide a target area with high oil concentration (see Section 4.3.5). The echosounder measured high acoustic backscatter within the dispersed oil plume (see Figure 34). The ability to detect a plume of oil in the water column could be useful when responding to ongoing releases, such as a subsea blowout. An echosounder was used in this application to successfully map an oil discharge plume under ice in a Canadian experimental spill in 1980 (Dickins and Buist, 1981).

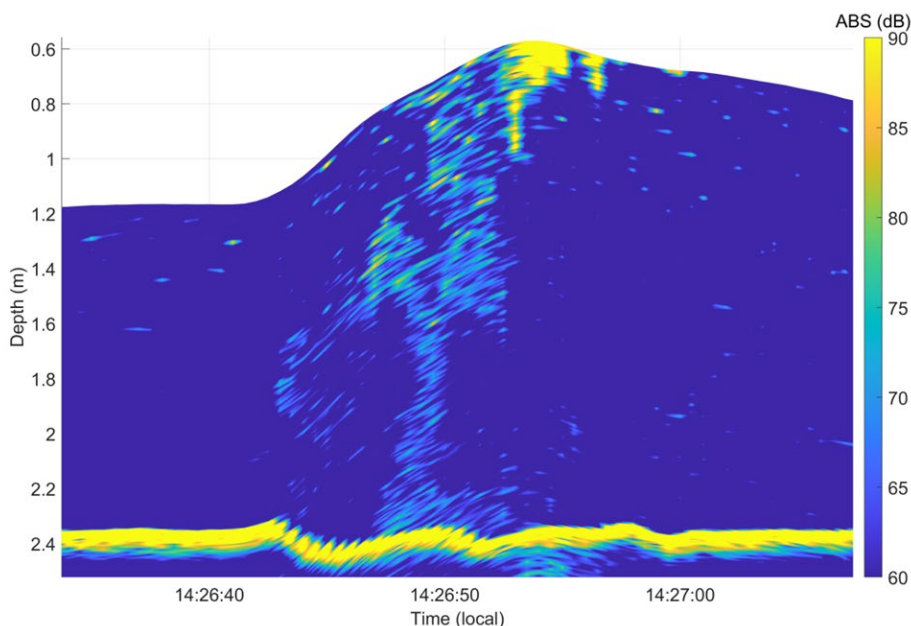
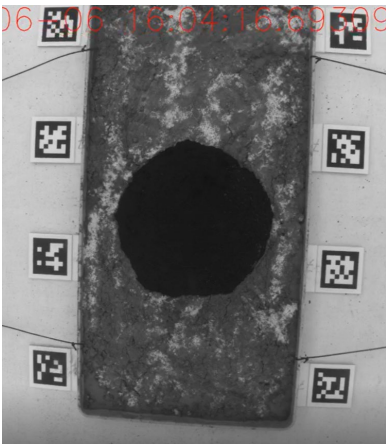


Figure 34: Echogram as Raven ROV passed through dispersed oil plume

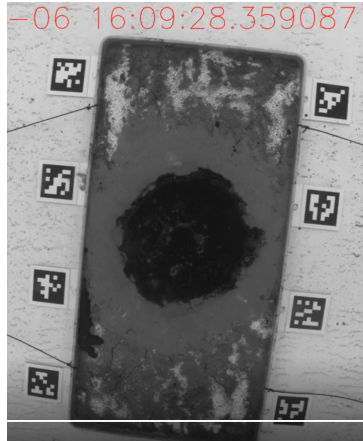
4.4.3 Camera

As at CRREL, the black and white camera provided clear images of the submerged oil pans (as seen in Figure 35) at all water depths (up to 2.4 m) under ambient daylight. Fine details were visible, even at some distance. However, the Ohmsett water is filtered and clear with no suspended particulates. The key discriminant for the visual data is visual contrast between the oil and the substrate, reinforced by the shape of the oil as it sits on the substrate; these are strongly influenced by both the composition of the seafloor; the sand and cement mix used in this experiment does not represent the full diversity of seafloors found in regions of interest.

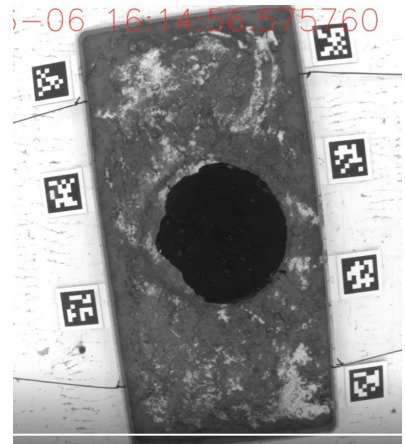
The camera should be useful in field conditions for providing context and orienting the platform relative to the target at short ranges. Reduced light with depth and in nighttime conditions will impact performance, but this may be offset by using floodlights, as demonstrated in Figure 36. Testing in the field to measure performance under more realistic turbidity, currents, light attenuation with depth, and greater distances from the seafloor is recommended.



Test Pan 7



Test Pan 10



Test Pan 12

Figure 35: Monochrome camera images of selected test pans

Test Pan 7 contained roofing tar, Test Pan 10 contained Tesoro decant oil, and Test Pan 12 contained in situ burn residue.

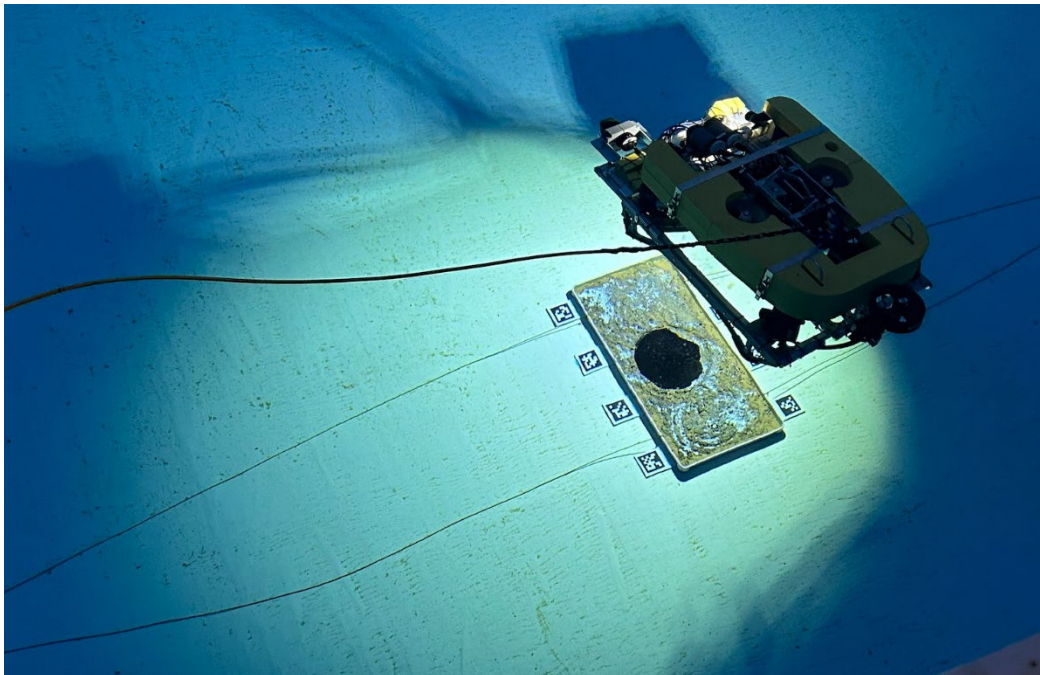


Figure 36: Nighttime operation of Raven ROV with LED floodlights

4.4.4 PAR

The PAR measurements from one pass of the Raven ROV down the tank, over the test pans, are shown in Figure 38. Note that the collimator was removed from the PAR on the Raven ROV due to it trapping air and causing buoyancy issues, and so the measurements are two orders of magnitude higher than during the tests at CRREL (see Section 3.4.4). The measurements show minima corresponding to the test pans, and maxima corresponding to the tank floor.

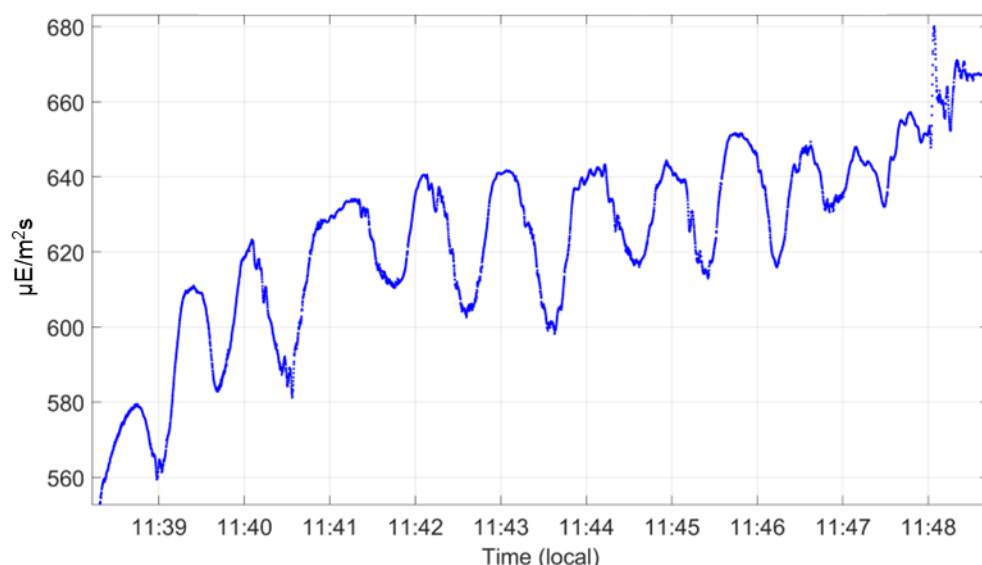


Figure 37: PAR measurements from Raven ROV pass over test pans

As was done with the echosounder measurements (see Section 4.4.2) the position of the PAR sensor relative to the test pans was determined using the monochrome camera images and the fiducial tags. The PAR results from a pass down the tank by the Raven ROV are shown in Figure 38. Lower PAR measurements (shown as darker red) corresponded to the center of the test pans with exposed oil deposits (i.e., Test Pans 4, 6, 7, 9, and 11). The empty test pans (Test Pans 2 and 3) and Test Pan 8, which had a layer of sand on top of the oil, showed higher and more even PAR measurements. This is an example of how the PAR results could be combined with positional data to scan and map an area.

Note that the contrast between the tank floor and the oil pools is large at Ohmsett, which makes detecting the oil much easier. Real seafloors would not be so reflective, and light attenuation with depth and water clarity would further impede this method; however the data validates the detection principle, and the results are encouraging for the potential use of the PAR sensor as a direct indicator of changes in reflected ambient light associated with the presence of oil residue on the seafloor. Further testing with more realistic bottom conditions would help clarify how useful the PAR would be in the field.

4.4.5 UV Fluorometer

The project team recognized early on that using the UV fluorescence sensor (Chelsea Technologies UviLux) in closed tanks such as CRREL and Ohmsett – that regularly test with oil and thus may have fugitive oil and elevated background concentrations – could be challenging, and the oil released by the relatively small test samples could be difficult to detect. Measurements made under ice but near the bottom of the CRREL tank showed little signal from the UV fluorometer (see Section 5.4.5).

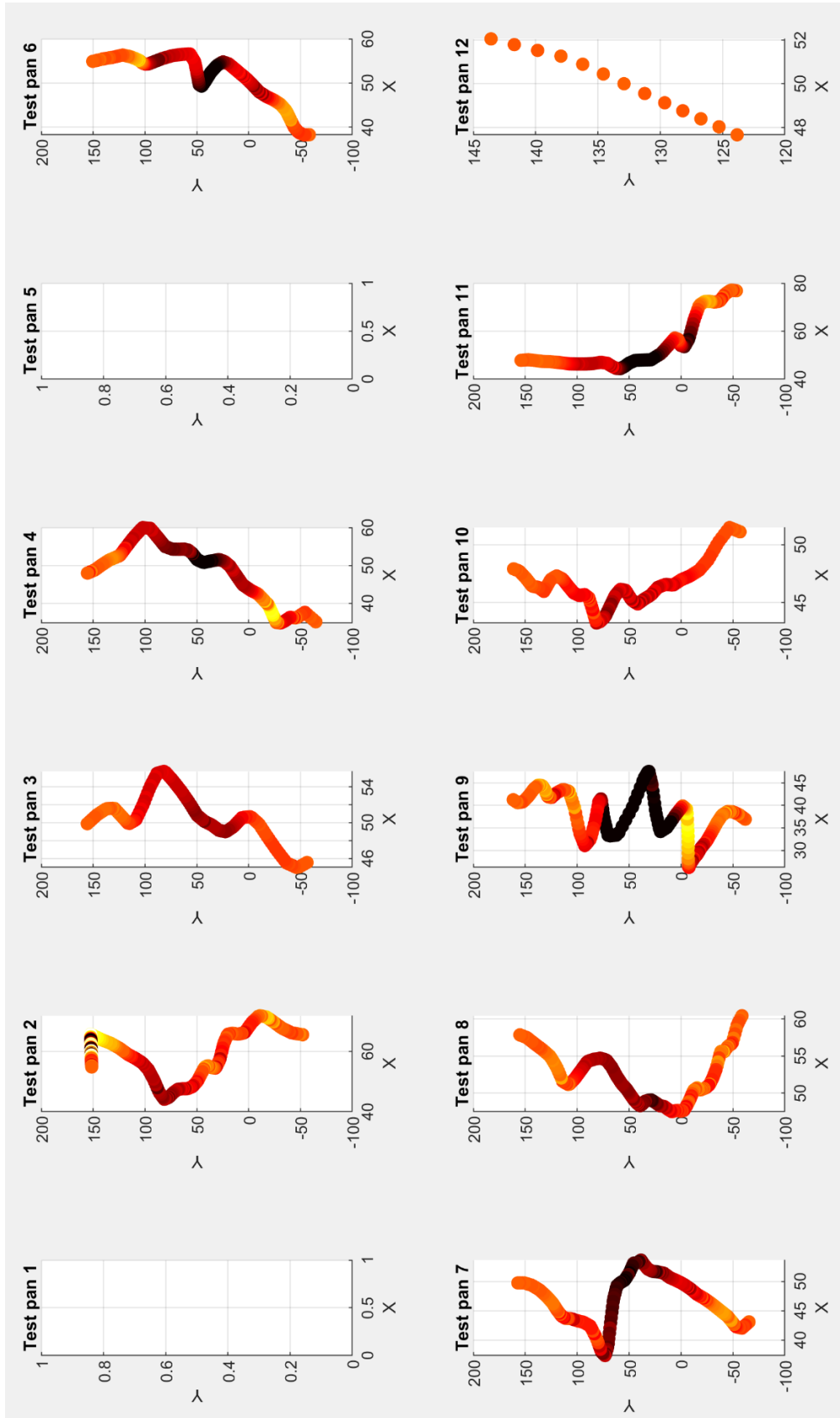


Figure 38: PAR measurements from Mission 8 transit of Raven ROV
 Test Pans 1 and 5 did not have fiducial tags and relative PAR position was not calculated.

Figure 39 shows the UV fluorescence measurements from several passes down the tank with the Remus 100 AUV. The background concentration of PAHs measured in the tank was approximately 2 µg/L. Several spikes in concentration above 25 µg/L were measured that could be associated with proximity to the test pans with oil, but corroborating measurements to confirm the source (e.g., water sampling and analysis near the Remus 100 AUV during transit, or dye tracer tests) were not taken.

The Raven ROV made similar passes down the tank; UV fluorescence measurements from the Raven ROV showed similar background concentrations as on the Remus 100 AUV, but the spikes were lower (maximum approximately 10 µg/L). The thrusters on the larger ROV could conceivably have disturbed dissolved oil in water above the sample trays and mixed or diverted those waters away from the UV fluorescence sensor, reducing spike amplitude.

Near the end of the experiment, oil was dispersed into the tank to create a region of high oil concentration. Two liters of HOOPs crude oil and 400 mL of Corexit 9500A were mixed into approximately 15 L of tank water with an electric stirrer and then pumped into the tank with an electric peristaltic pump. The oil dispersed into several large patches that were visible to observers and the Raven ROV camera (see Figure 40).

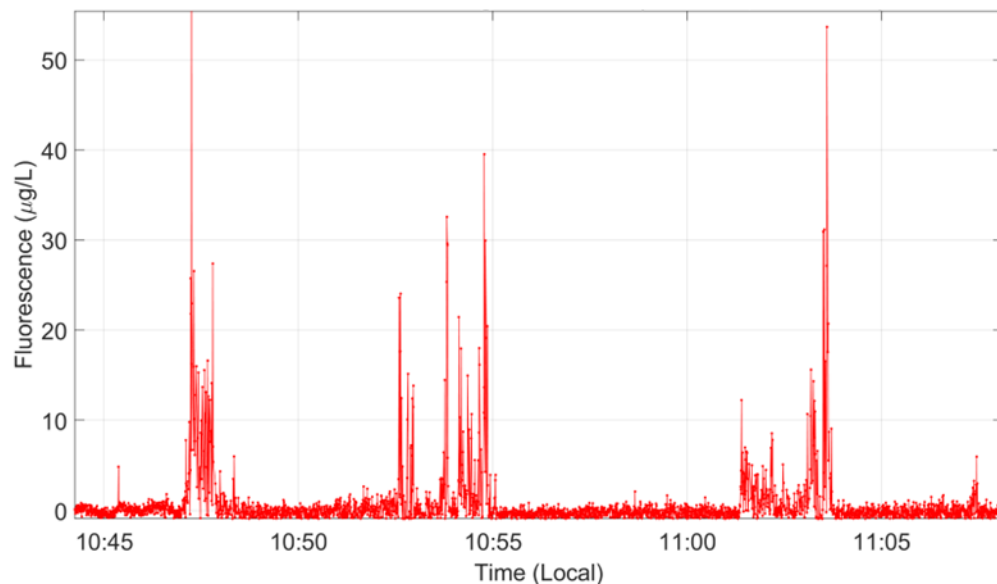


Figure 39: UV Fluorescence measurements from Remus 100 AUV

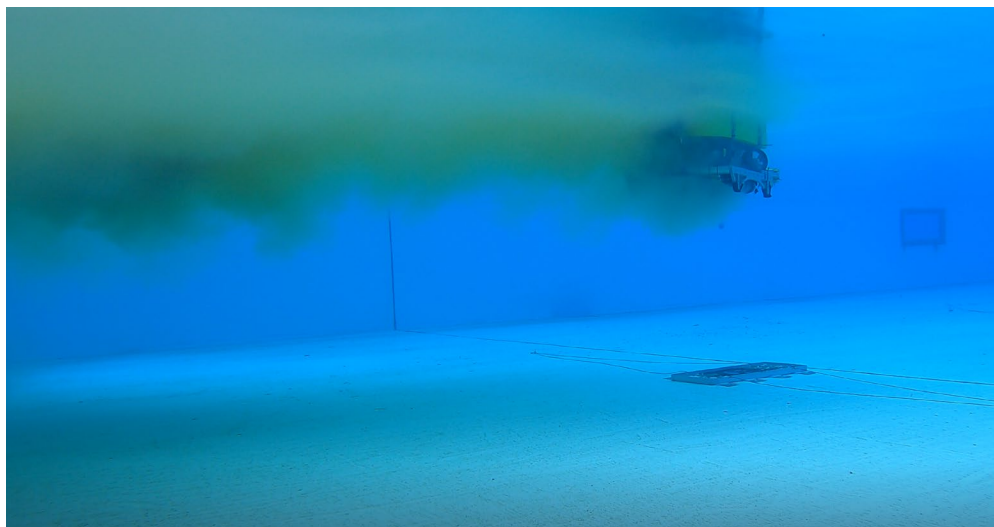


Figure 40: Raven ROV traversing dispersed oil plume

This permitted the position of the Raven ROV (i.e., in or out of the dispersed oil cloud) to be directly compared with the UV fluorescence measurements, to verify that the UV fluorometer was responding appropriately. The UV fluorometer showed good responsiveness as the Raven ROV moved in and out of the dispersed oil cloud, at times reading maximum detectable concentrations (see Figure 41). This result provided more confidence that the concentrations spikes in Figure 39 were from the dissolved oil from the test pans and not from residual oil from previous tests at Ohmsett.

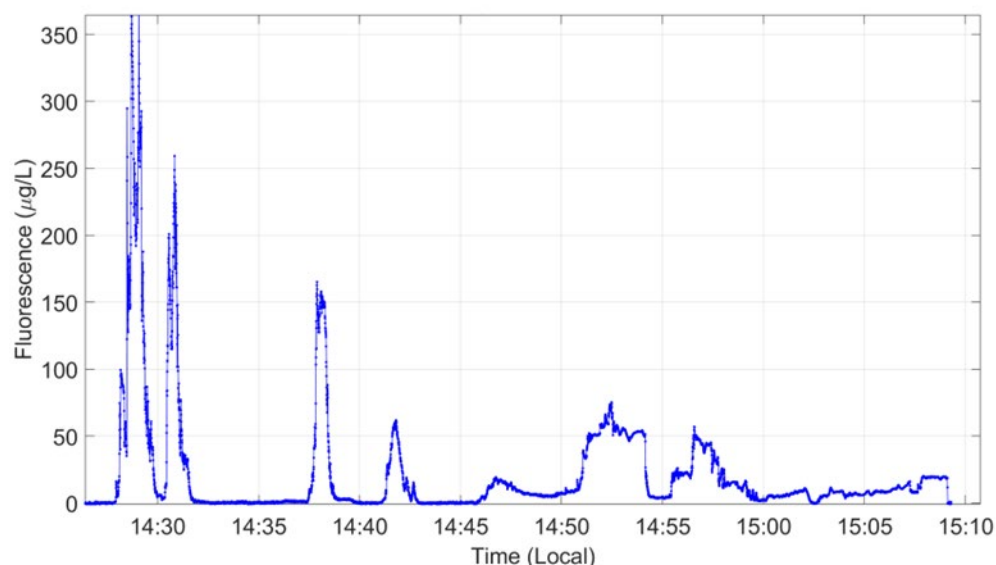


Figure 41: UV Fluorescence measurements of dispersed oil plume

5 Conclusions

The conclusions from the tests to detect oil under ice tests at CRREL are summarized below:

- Oil pools under ice were detected by the echosounder, PAR, and cameras while stationary and while moving at up to 0.5 m/s.
- The echosounder was able to discriminate between the ice sheet and oil layers thicker than approximately 1 cm; the results were consistent with previously reported acoustic-based studies.
- The imaging sonar produced clear images of the underside of the ice sheet, but the oil pools did not appear significantly different from the surrounding areas; the small size of the tank limited the ability to test the imaging sonar.
- Some interference was noted between instrument signals when they operated simultaneously, for example the imaging sonar and the echosounder; this could be managed by sequentially triggering the sensors.
- The ability to test the UV Fluorometer was limited due to the tank being a closed system with relatively high background concentrations; however, a 10% increase in average concentration was measured after oil was added to the Test Areas.
- It was not possible to encapsulate the oil pools in ice in the time available at CRREL.

The conclusions from the tests to detect submerged oil at Ohmsett are summarized below:

- The imaging sonar produced clear images of the tank and test pans, and the heavy oil samples showed different acoustic reflectivity from the surrounding sand.
- The echosounder data showed identifiable differences in reflectivity between the roofing tar samples and the underlying sand, but the differences in reflectivity with the Tesoro Decant Oil and burn residue samples were not as defined.
- The monochrome camera provided clear images of the tank bottom, test pans, and heavy oil samples.
- The PAR registered differences in reflected light intensity when passing over the pans and heavy oil samples, compared to the tank bottom.
- The UV fluorometer registered small increases in PAH concentration in the vicinity of the sample pans, particularly in the data collected by the Remus 100 AUV.

Comparing the data from multiple sensors that are interrogating different points in space due to their orientation or operating principle, while the platform is moving in three dimensions, is complex. Combining data streams from all sensors to facilitate comparison can be done if navigation records are sufficiently accurate, but this requires time to process. The comparison is made more complex if the data requires interpretation, for example identifying different mediums (e.g., oil, ice, substrate) on an echogram. Developing a methodology to combine sensor streams will require high-quality data gathered from realistic simulated spills.

Table 13 presents a qualitative ranking of the ability of the selected sensors to detect oil located i) under ice and ii) submerged on a sandy substrate, based on the tests completed to date.

Table 13: Qualitative performance of sensors to detect oil

Sensor	Oil Under Ice	Submerged Oil
Imaging Sonar	Uncertain	High
Echosounder	High	Uncertain
Camera	High	Medium*
PAR	High	Medium*
UV Fluorometer	Uncertain	Medium

*subject to water clarity and light attenuation

6 Recommendations

Testing the sensor package in test basins was a necessary and important step in developing a remote system that could be deployed at a spill. The results of the basin tests showed that the sensor results could collectively identify oil in the test areas. However, there are significant differences between conditions at CRREL and Ohmsett, and what is expected at a real spill that would affect the performance of the sensors. For example,

- Distances between sensors and targets were limited by the depth of the tanks, and they were much closer to the oil
- The hard surfaces and right angles in tanks strongly reflect acoustic signals and there may be less interference from the irregular and softer boundaries in natural water bodies
- Tanks have painted surfaces that evenly reflect light and relatively clear water compared to natural ocean floors and turbidity
- Natural ice in the winter will vary in salinity, internal crystal structure, thickness, small-scale and large-scale bottom roughness, clarity, and surface cover (e.g., snow drifts) more than the ice sheet grown at CRREL under unusually warm conditions
- Background hydrocarbon concentrations from previous tests with oil at CRREL and Ohmsett were high relative to what is expected in the field (at least outside the immediate spill area) and masked the effects from the test oils on the water quality
- CRREL was unable to grow a sufficiently thick ice layer underneath the oil targets in the two weeks of available tank time, and the effects of ice encapsulation on sensor performance could not be evaluated

A field trial in a natural environment is an important next step in developing and proving the sensor package. Research questions that would be addressed by a field trial are summarized in Table 14.

Table 14: Field trial research questions

Sensor Principle	Oil Under Ice	Submerged Oil
General	How will oil encapsulation affect performance of sensors?	
Acoustic	How will the large-scale roughness of natural ice affect acoustic backscatter and the ability to detect trapped oil pools?	How do different benthic substrates affect acoustic heavy oil detection?
Optical	How will natural variations in ice thickness, structure, clarity, and surface covering affect ability of PAR and cameras to detect oil?	How will appearance of oil targets differ from natural bottom materials?
	How will water depth and clarity affect operation of PAR and cameras, and distances from targets they will be effective?	How will depth and water clarity affect ability of PAR and cameras to detect submerged oil?

	Can onboard strobes substitute for daylight for nighttime or low-light operations with varying snow cover?	Will PAR detect changes in reflected daylight or artificial light between natural bottom materials and submerged oil?
Fluorometry	Will fluorometer detect PAH or BTEX from oil under ice or oil encapsulated in ice above background concentrations?	Will fluorometer detect PAH or BTEX from submerged oil above background concentrations?

6.1 Field Trial Design Considerations

The field trial should be conducted in two phases: an open-water phase that tests with submerged oil, and an ice phase that tests with oil under and encapsulated in ice. The submerged oil phase should include:

- Evaluating the ability of the sensor package to detect larger submerged oil targets (heavy oil/Bunker C, in situ burn residue, and possibly a weathered dilbit) at several locations with varying depth and bottom characteristics (rocky and soft organic-laden sediments).
- Evaluating different AUV survey patterns to intersect and map the boundary of oil contamination at an operational scale, not possible in a confined tank setting

The oil under ice phase should include:

- Evaluating the ability of the sensor package to detect oil pools trapped under ice and encapsulated within ice.
- The use of a crude oil substitute that would have similar properties to crude oil for some of the sensor principles, such as dyed vegetable oil, to simulate larger pools of oil.
- Evaluating the ability of the sensor package to detect and map oil under ice and oil encapsulated within ice without the artificial scale constraints and artificial surface interferences imposed by test basins.
- Gathering navigational data with the AUV to assist with winter deployment, operations (i.e., deployment and retrieval) under ice at a scale that more closely reflects a real event.

Testing in the field with natural ice and snow would provide critical information on background variation in light transmission to compare with the tank PAR and camera results, and permit testing the sensors at longer ranges.

7 References

[API] American Petroleum Institute. 2016. Sunken Oil Detection and Recovery. API Technical Report 1154-1.

Bassett C, Lavery AC, Maksym T and Wilkinson JP. 2014. Laboratory measurements of high-frequency, acoustic broadband backscattering from sea ice and crude oil. *The Journal of the Acoustic Society of America*, 137(1), EL32-EL38.

Bassett C, Lavery AC, Maksym T and Wilkinson JP. 2016. Broadband acoustic backscatter from crude oil under laboratory-grown sea ice. *The Journal of the Acoustic Society of America*, 140(4), pp 2274-2287.

Bello JM, Eriksen P, and Pocwiardowski P. 2016. Oil Leak Detections with a Combined Fluorescence Polarization Instrument and a Wide Band MultiBeam Sonar: Phase II Final Report.

Bradford JH, Marshall HP, Babcock E, and Dickins D. 2015. Targeted Full-Waveform Inversion of Ground Penetrating Radar Data for Quantification of Spills Under Sea ice. *Proceedings Offshore Arctic Technology Conference*, Copenhagen, Denmark.

Bradford JH, Dickins DF, and Brandvik PJ. 2010. Detection of snow-covered oil spills on sea ice using ground-penetrating radar. *Geophysics* 75:G1-G12, doi: 10.1190/1.3312184.

Buist I, Trudel K, Morrison J, and Aurand D. 1997. Laboratory Studies of the Properties of In-Situ Burn Residues. *Proceedings of the 1997 International Oil Spill Conference*, pp 149-156.
CSE, 2014. *Scientific Style and Format: the CSE Manual for Authors, Editors, and Publishers*. 8th Edition. 840 p.

Dickins DF. 2017. Arctic Oil Spill Response Technology Joint Industry Programme Synthesis Report. Final report to the International Association of Oil and Gas Producers (IOGP) Arctic Oil Spill Response Technology Joint Industry Programme (JIP), 106 pp.

Dickins DF, Andersen JH, Brandvik PJ, Singsaas I, Buvik T, Bradford J, Hall R, Babiker M, Kloster K, and Sandven S. 2010. Remote Sensing for the Oil in Ice Joint Industry Program. *Proceedings 33rd Arctic and Marine Oil Spill (AMOP) Technical Seminar*, Environment Canada, Ottawa, ON.

Dickins D, Brandvik PJ, Bradford J, Faksness LG, Liberty L, and Daniloff R. 2008. Svalbard 2006 Experimental Oil Spill under Ice: Remote Sensing, Oil Weathering Under Arctic Conditions and Assessment of Oil Removal by In-situ Burning. *Proceedings International Oil Spill Conference*, American Petroleum Institute. Washington, DC.

Dickins DF, Liberty L, Hirst W, Bradford J, Jones V, Zabilansky L, Gibson G, and Lane J. 2005. New and Innovative Equipment and Technologies for the Remote Sensing and Surveillance of Oil in and Under Ice. *Proceedings 28th Arctic and Marine Oil spill Program (AMOP) Technical Seminar*, Environment Canada, Ottawa ON.

Dickins DF. 2011. Behavior of oil spills in ice and implications for Arctic spill response. Paper No. OTC22126, Proceedings Arctic Technology Conference, Houston TX.
<https://dfdickins.com/pdf/OTC22126LR.pdf>

Dickins DF. 2000. Detection and Tracking of Oil under Ice. Report prepared for the US Department of Interior, Minerals Management Service, Herndon VA.

Dickins DF and Buist IA. 1999. Oil Spill Countermeasures for Ice-covered Waters. *Journal of Pure and Applied Chemistry* 71(1): L173-L191.

Dickins DF and Buist IA. 1981. Oil and Gas Under Sea Ice Study. Proceedings International Oil Spill Conference, Atlanta, GA.

Dollhopf RH, Fitzpatrick FA, Kimble JW, Capone DM, Graan TP, Zelt RB, and Johnson R. 2014. Response to Heavy, Non-Floating Oil Spilled in a Great Lakes River Environment: A Multiple-Lines-Of-Evidence Approach for Submerged Oil Assessment and Recovery. Proceedings of the 2014 International Oil Spill Conference. American Petroleum Institute, Washington, D.C., pp 434-448.

[Enbridge] Enbridge Gas Inc. 2021. Making things right: A Marshall response timeline. Retrieved from www.enbridge.com/marshall-release-timeline.

Fingas MG and Brown CE. 2017. Oil Spill Remote Sensing Technologies, Proceedings of the Fortieth AMOP Technical Seminar, Environment and Climate Change Canada, Ottawa, ON, pp. 82-117.

Giodini S, van der Spek E, and Dol H. 2015. Underwater Communications and the Level of Autonomy of AUVs: a Tale of Two Technologies. *Hydro International*

Hansen KA, Fitzpatrick M, Herring PR, and VanHaverbeke M. 2009. Heavy Oil Detection (Prototypes) – Final Report. Report No. CG-D-08-09.

Leifer I, Lehr WJ, Simecek-Beatty D, Bradley E, Clark R, Dennison P, Hu Y, Matheson S, Jones CE, Holt B, Reif M, Roberts DA, Svejksky J, Swayze G, and Wozencraft JI. 2012. State of the art satellite and airborne marine oil spill remote sensing: Application to the BP Deepwater Horizon oil spill. *Remote Sensing of Environment* 124:185-209.
<https://www.sciencedirect.com/science/article/abs/pii/S0034425712001563>

[NASEM] National Academies of Sciences, Engineering, and Medicine. 2022. Oil in the Sea IV: Inputs, Fates, and Effects. Washington, DC: The National Academies Press.
<https://doi.org/10.17226/26410>.

Owens EH and Dickins DF. 2015. Guide to Oil Spill Response in Snow and Ice Conditions, Arctic Council, Prepared for Emergency Prevention, Preparedness and Response Group, Tromsø.

Pegau W, Garron J, and Zabilansky L. 2016. Detection of Oil on-in-and-under-ice. Final report to the International Association of Oil and Gas Producers (IOGP) Arctic Oil Spill Response Technology Joint Industry Programme (JIP), 406 pp.

Pocwiardowski P. 2017. SpiDeR – Spill Detection and Recognition System for ROV Operations. Proceedings of the 2021 International Oil Spill Conference.

Shigenaka G, Meyer B, Overton E, and Miles MS. 2017. Physical and Chemical Characterization of In-situ Burn Residue Encountered by a Deep-Water Fishery in the Gulf of Mexico. Proceedings of the 2017 International Oil Spill Conference, pp 185-195.

Wang Y, Thanyamanta W, Bulger C, Bose N, and Brown R. 2022. An Experimental Study of The Cooperation Between Sonar and a Fluorometer for Detecting Underwater Oil from an Underwater Vehicle. Oceans.

Watkins RK, Allen AA, and Ellis BC. 2016. Remote Sensing Guide to Oil Spill Detection in Ice-Covered Waters. Arctic Oil Spill Response Technology Joint Industry Programme.

Wilkinson JP, Boyd T, Hagen B, Maksym T, Pegau S, Roman C, Singh H, and Zabilansky L. 2015. Detection and quantification of oil under sea ice: The view from below. Cold Regions Science and Technology, Vol. 109: 9-17.

Appendices

Appendix A: Technical Summary

REPORT TITLE: Detection of Oil Under Ice and On the Seafloor

CONTRACT NUMBER(S): 140E0122C0008

FISCAL YEARS(S) OF PROJECT FUNDING: FY2022 to FY2025

CUMULATIVE PROJECT COST: 1,218,526

COMPLETION DATE OF REPORT: 30 April 2025

BSEE COR(S): Dr. Jay Cho

BSEE CO(S): Tae-Won Eum

PROJECT MANAGER(S): James McCourt

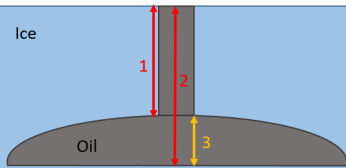
AFFILIATION OF PROJECT MANAGER: SL Ross Environmental Research Ltd.

ADDRESS: 200-38 Auriga Drive, Ottawa, ON, K2E 8A5

PRINCIPAL INVESTIGATOR(S)*: James McCourt

KEY WORDS: remote sensing, submerged and sunken oil, oil in ice

Appendix B: CRREL Ice Core Data

North Core - 2/7/24 @ 1500									
Depth of Ice	Temperature	Salinity (ppt)	Density (g/mL)		North Core Density Calc				
5 cm	-1.5	4.6	0.993		Depth	Length (cm)	Diameter (cm)	Weight (g)	Volume (cm ³)
10 cm	-1.6	5.9			0 - 10 cm	9.936	7.296	412.7	415.40
15 cm	-2.1	5.2	0.971		10 - 20 cm	8.033	7.252	322.2	331.81
20 cm	-2.0	5.1			20 - 30 cm	9.641	7.094	370.48	381.06
25 cm	-1.6	4.8	0.972		30 - 40 cm	8.272	7.208	305.49	337.54
30 cm	-1.4	4.3							
35 cm	-1.3	5.3	0.905						
*total Ice thickness = 39 cm		*Skeletal Layer thickness = 3 cm							
Mid Core - 2/7/24 @1520									
Depth of Ice	Temperature	Salinity (ppt)	Density (g/mL)		Mid Core Density Calc				
5 cm	-1.8	5.9	1.005		Depth	Length (cm)	Diameter (cm)	Weight (g)	Volume (cm ³)
10 cm	-2.1	5.7			0 - 10 cm	9.65	7.139	388.36	386.27
15 cm	-2.8	5.8	0.981		10 - 20 cm	10.65	7.325	440.39	448.80
20 cm	-2.6	5.8			20 - 30 cm	11.075	7.224	419.26	453.93
25 cm	-2.5	5.8	0.924		30 - 40 cm	9.895	7.313	385.6	415.62
30 cm	-2.3	5.4			40 - 50 cm	6.742	6.893	231.27	251.59
35 cm	-2.2	4.9	0.924						
40 cm	-2.1	4.4							
45 cm	-1.9	6.4	0.919						
*total Ice thickness = 49 cm		*Skeletal Layer thickness = 3 cm							
South Core - 2/7/24 @1420									
Depth of Ice	Temperature	Salinity (ppt)	Density (g/mL)		South Core Density Calc				
5 cm	-1.1	5.7	1.001		Depth	Length (cm)	Diameter (cm)	Weight (g)	Volume (cm ³)
10 cm	-1.7	5.0			0 - 10 cm	9.429	7.884	460.58	460.31
15 cm	-1.6	5.0	0.940		10 - 20 cm	9.951	7.333	395.15	420.26
20 cm	-1.2	4.8			20 - 30 cm	9.559	7.24	324.37	393.53
25 cm	-1.9	4.6	0.824		30 - 40 cm	9.738	7.306	345	408.24
30 cm	-1.5	4.5							
35 cm	-1.6	6.3	0.845						
*total Ice thickness = 39 cm		*Skeletal Layer thickness = 3 cm							
Control Core - 2/9/24 @0845									
Depth of Ice	Temperature	Salinity (ppt)	Density (g/mL)		Control Core Density Calc				
5 cm	-2.5	5.7	0.963		Depth	Length (cm)	Diameter (cm)	Weight (g)	Volume (cm ³)
10 cm	-2.3	4.8			0 - 10 cm	9.823	7.333	399.64	414.86
15 cm	-2.1	5.3	0.920		10 - 20 cm	9.933	7.274	379.55	412.78
20 cm	-2.0	4.2			20 - 30 cm	7.755	7.974	301.4	387.28
25 cm	-1.8	6.2	0.778						
*total Ice thickness = 28 cm		*Skeletal Layer thickness = 3 cm							
Cores from After Testing 2/15/24									
Location	Ice Thickness	Surf. to Bot.	Oil Thickness (cm)		<div><div>Ice Surface</div><div></div><div>Water</div><div>1 – Core Thickness 2 – Surface of Ice to Bottom of oil 3 – Oil Thickness</div></div>				
North	35								
Mid (between 3	35								
South	44								
Pad 1*	56.5								
Pad 2*	23	24.5	1.5						
Pad 3*	23	25	2						
Pad 4*	24.5	27	2.5						
Pad 5*	24	28	4						
Pad 6*	26	32.5	6.5						
*measurements taken 3/4/24 - 2 weeks after completion of testing to allow for ice growth underneath oil pockets									

Appendix C: CRREL Test Matrix and Mission Summary

	BSEE CRREL (February 2024)			Oil under ice					
MISSIONS	Timing			Custom BSEE payload					Description
	Date (local)	Start	End	Camera	BlueView	PAR	Sig1000	UVLux	
'Cart'									
5	2024-02-06	13:35	14:54	n	y	n	n	n	test matrix
6	2024-02-06	15:01	15:34	y	n	y	n	n	test matrix
7	2024-02-06	16:00	16:13	y	n	y	n	n	test matrix, PAR with collimator
8	2024-02-07	10:20	14:49	y	n	y	y	y	test matrix
9	2024-02-07	15:01	17:00	y/n	y/n	y/n	y	y/n	test matrix
10	2024-02-08	8:45	11:20	y/n	y/n	y/n	y/n	y/n	finish test matrix, pumps ON/OFF
11	2024-02-08	12:19	15:52	y	n	y	y	y	inject oil pad 6
12	2024-02-08	16:00	8:26	y	n	y	y	y	overnight
13	2024-02-09	9:36	10:20	y	n	y	y	y	inject pad 5
14	2024-02-08	10:27	11:12	y	n	y	y	y	inject pad 4
15	2024-02-09	11:16	11:40	y	n	y	y	y	inject pad 3
16	2024-02-09	11:48	11:54	y	n	y	y	y	inject pad 2
17	2024-02-09	12:14	13:00	y	n	y	y	y	under pad 2
18	2024-02-09	13:11	13:38	y	n	y	y	y	all pads with oil
19	2024-02-09	13:45	14:01	y	n	y	y	y	Sig1000 with pulse compression
20	2024-02-09	14:10	14:24	y	n	y	y	y	all pads
21	2024-02-09	14:30	15:47	y	y	y/n	n	y/n	
22	2024-02-09	16:00		y	n	y	y	y	over weekend
23	2024-02-12	9:12	9:30	y	y/n	y	y/n	y	waiting on oil encapsulation, overnight
24	2024-02-13	9:30	15:17	y	y/n	y	y/n	y	
25	2024-02-13	15:17	11:58	y	n	y	y	y	overnight, cov er off next day
26	2024-02-14	12:23	13:26			y/n			camera stopped
27	2024-02-14	13:57		y	y/n	y	y/n	y	
28	2024-02-14	14:25	17:02	y/n	n	y	y	y/n	Sig1000 pulse compression
29	2024-02-14	17:09	17:38	y	n	y	y	y	test matrix
30	2024-02-14	18:27	19:20	y	n	y	y	y	nighttime
31	2024-02-14	19:29		y	n	y	y	y	overnight
32	2024-02-15	9:11	9:50	y	n	y	y	y	test matrix
33	2024-02-15	9:53	9:56	y/n	y/n	y/n	y	y/n	Sig1000 pulse compression
34	2024-02-15	10:03	11:21	y/n	y/n	y/n	y/n	y/n	finished test matrix
UTC = local + 4 hr									

Appendix D: Ohmsett Test Matrix and Mission Summary

BSEE OHMSETT (3-7 June 2024)				Sunken oil											
MISSIONS	Date (UTC)	Timing		Frontseat payload				Custom BSEE payload				Description			
		Start	End	YSI CTD	EOCPuck	Optode	Sig1000's	Camera		BlueView	PAR	UMLux			
ROV 'Raven'															
1	2024-06-04	20:15	20:48	n/a	n/a	n/a	y	y	n	y	y	y	Vehicle test, calibrations, hover over tray		
2	2024-06-04	21:16	21:35	n/a	n/a	n/a	y	y	n	y	y	y	Vehicle test, hover near tray 6		
3	2024-06-05	16:09	17:10	n/a	n/a	n/a	y	partial	y	y	y	n	Survey of all trays, some video loss		
4	2024-06-05	17:27	18:48	"	"	"	y	partial	n	y	y	y	Test matrix 3, 1m altitude		
5	2024-06-05	19:01	19:23	"	"	"	y	y	n	y	y	y	Hovering over trays		
6	2024-06-05	20:42	21:10	"	"	"	y	y	y	y	y	y	Test matrix 4, 3		
7	2024-06-05	23:26	0:45	"	"	"	y	y	n	y	y	y	Nighttime test matrix 9, 10		
8	2024-06-06	14:59	16:23	"	"	"	y	y	y	y	y	y	Test matrix 4, 3, 5, then survey trays 12, 10,		
9	2024-06-06	17:29	17:40	"	"	"	y	y	n	y	y	y	Survey of all trays		
10	2024-06-06	17:40	18:16	"	"	"	y	y	n	y	y	y	3D mapping of trays 3, 7, 10, 12		
11	2024-06-06	18:17	19:09	"	"	"	y	y	y	y	y	y	Dispensed oil plume		
AUV 'NGR'															
277	2024-06-05	14:10	16:20	n	n	n	y	y	y	y	y	y	First trials, towed by lines		
277	2024-06-05	15:23	15:27	y	y	y	y	y	y	y	y	y	Towed by lines at surface, frontseat active		
278	2024-06-06	13:28	14:54	n	n	n	y	y	y	y	y	y	Surface run alongside dinghy		
278	2024-06-06	14:03	14:12	y	y	y	y	y	y	y	y	y	Attempt at subsurface run, towed by lines, frontseat active		



Department of the Interior (DOI)

The Department of the Interior protects and manages the Nation's natural resources and cultural heritage; provides scientific and other information about those resources; and honors the Nation's trust responsibilities or special commitments to American Indians, Alaska Natives, and affiliated island communities.



Bureau of Safety and Environmental Enforcement (BSEE)

The mission of the Bureau of Safety and Environmental Enforcement works to promote safety, protect the environment, and conserve resources offshore through vigorous regulatory oversight and enforcement.

BSEE Oil Spill Preparedness Program

BSEE administers a robust Oil Spill Preparedness Program through its Oil Spill Preparedness Division (OSPD) to ensure owners and operators of offshore facilities are ready to mitigate and respond to substantial threats of actual oil spills that may result from their activities. The Program draws its mandate and purpose from the Federal Water Pollution Control Act of October 18, 1972, as amended, and the Oil Pollution Act of 1990 (October 18, 1991). It is framed by the regulations in 30 CFR Part 254 – *Oil Spill Response Requirements for Facilities Located Seaward of the Coastline*, and 40 CFR Part 300 – *National Oil and Hazardous Substances Pollution Contingency Plan*. Acknowledging these authorities and their associated responsibilities, BSEE established the program with three primary and interdependent roles:

- Preparedness Verification,
- Oil Spill Response Research, and
- Management of Ohmsett - the National Oil Spill Response Research and Renewable Energy Test Facility.

The research conducted for this Program aims to improve oil spill response and preparedness by advancing the state of the science and the technologies needed for these emergencies. The research supports the Bureau's needs while ensuring the highest level of scientific integrity by adhering to BSEE's peer review protocols. The proposal, selection, research, review, collaboration, production, and dissemination of OSPD's technical reports and studies follows the appropriate requirements and guidance such as the Federal Acquisition Regulation and the Department of Interior's policies on scientific and scholarly conduct.